Nonpairwise Interactions Induced by Virtual Transitions in Four Coupled Artificial Atoms

M. Schöndorf* and F.K. Wilhelm
Theoretical Physics, Saarland University, 66123 Saarbrücken, Germany

(Received 4 June 2019; revised manuscript received 26 September 2019; published 10 December 2019)

Various protocols implementing a quantum computer are being pursued, one of which is the adiabatic quantum computer. Natural interactions in electromagnetic environments are only two-body local interactions, but the construction or simulation of higher-order couplers is indispensable for a universal adiabatic quantum computer using conventional flux qubits (no nonstoquastic interactions). Here we show that in a specific flux-qubit coupler design without ancilla qubits, four-body stoquastic interactions are induced by virtual coupler excitations. For specific parameter regimes they are the leading effect and can be tuned up to the gigahertz range.

DOI: 10.1103/PhysRevApplied.12.064026

I. INTRODUCTION

Quantum computers have the potential to lead to an exponentially reduced computation time compared with classical computers for certain problems. One promising candidate for the realization of such a device is an adiabatic quantum computer (AQC), where the computation proceeds from an initial Hamiltonian whose ground state is easy to prepare to the ground state of a final Hamiltonian that encodes the solution of the computational problem, by avoiding excitations [1–4]. It has been shown that an AQC an be used for universal quantum computing [5]. Still, implementing an AQC with verifiable speedup is a difficult task. A big step is to overcome the locality of natural interactions. k local interactions with $k > 2$ are suitable for the effective implementation of various optimization algorithms [6]. Furthermore, since conventional qubit designs are not feasible to implement nonstoquastic interactions [7,8], a logical way to establish universality in AQCs is to realize interactions with $k > 2$ [9]. There are embedding schemes that simulate this type of coupling requiring a large overhead, such that it would be desirable to implement them as natively as possible. Furthermore higher-order local interactions are interesting from a fundamental-physics point of view since the only known and proven interaction between more than two particles is found in Efimov states [10,11].

There are many proposals to realize higher-local interactions, using quantum embedding or ancilla qubits [12–14], which all create a huge overhead. In this paper we propose a specific coupler architecture using flux qubits [15] and prove the existence of four non-negligible antiferromagnetic four-body interactions.

In Sec. II we present the system of interest and derive the corresponding Hamiltonian. The numerical and analytical results are presented in Sec. III. In Sec IV we discuss the effect of flux noise and in Sec. V we give our conclusion.

II. SETUP AND HAMILTONIAN

In our setup, four qubits are connected via a nonlinear coupler (see Fig. 1). Here the qubits as well as the nonlinear coupler are realized by an inductive loop with inductivity L_j interrupted by a Josephson junction with capacity C_j and critical current $I_j^{(c)}$; namely, a flux qubit. The junction represents the nonlinear ingredient of the system. Here $j \in \{1, 2, 3, 4, c\}$. A crucial point is that the coupler's plasma frequency has to be chosen higher than the qubit plasma frequencies to avoid transitions between coupler energy levels. The corresponding quantum variables are the quantized fluxes of the five loops $\hat{\Phi}_j$. The Hamiltonian describing Fig. 1 can be obtained by standard circuit quantization. We split the Hamiltonian into three parts [16]

$$\hat{H} = \sum_{j=1}^{4} \hat{H}_j + \hat{H}_c + \hat{H}_{\text{int}}, \tag{1}$$

the sum over the bare-qubit Hamiltonians $\hat{H}_j$, the bare-coupler Hamiltonian $\hat{H}_c$, and the interaction Hamiltonian H_{int}. The qubit and coupler Hamiltonians include a quadratic potential coming from the LC part and a cosine contribution form the Josephson junction. The strength of the nonlinear term is determined by the ratio between the Josephson energy $E_J = \Phi_0 I_j^{(c)}/2\pi$ and the inductive energy $E_{L_j} = (\Phi_0/2\pi)^2/L_j$, where Φ_0 denotes the flux

*marius.schoendorf@gmx.de

quantum. More interest should be paid to the interaction part, which arises from an induced external flux from the qubits to the coupler and vice versa. Furthermore, we operate the coupler as well as the qubits at (or close to) the flux degeneracy point. The different parts of Eq. (1) can be written in unitless parameters (for a detailed derivation see Appendix A):

$$\hat{H}_j = E_{L_j}\left(4\xi_j^2\frac{\hat{q}_j^2}{2} + (1+\alpha_j^2)\frac{\hat{\varphi}_j^2}{2} + \beta_j\cos\hat{\varphi}_j\right), \quad (2)$$

$$\hat{H}_c = E_{\tilde{L}_c}\left(4\xi_c^2\frac{\hat{q}_c^2}{2} + \frac{\hat{\varphi}_c^2}{2} + \beta_c\cos\hat{\varphi}_c\right), \quad (3)$$

$$\hat{H}_{\rm int} = E_{\tilde{L}_c}\left(\sum_{i<j}^{4}\alpha_i\alpha_j\hat{\varphi}_i\hat{\varphi}_j + \sum_{j=1}^{4}\alpha_j\hat{\varphi}_c\hat{\varphi}_j\right). \quad (4)$$

Here we rescale the coupler impedance $\tilde{L}_c = L_c - \sum_{j=1}^{4}\alpha_j M_j$ to decouple equations, where M_j denotes the mutual inductances of the jth qubit and $\alpha_j = M_j/L_j$ is the dimensionless mutual inductance. Additionally, we define the parameter $\xi_j = 4\pi Z_j/R_Q$ with characteristic impedance $Z_j = \sqrt{L_j/C_j}$ and the resistance quantum $R_Q = h/e^2$. The quantized phases are given by $\hat{\varphi}_j = (2\pi/\Phi_0)\hat{\Phi}_j + \pi$, and $\hat{q}_j$ is the conjugated quantum variable. We shift the phases that appear by π, leading to the positive sign in front of the cosine part. For the coupler and qubits, the screening parameter is given by $\beta_c = 2\pi\tilde{L}_c I_c^{(c)}/\Phi_0$ and $\beta_j = 2\pi L_j I_j^{(c)}/\Phi_0$, respectively, where $I_j^{(c)}$ denotes the critical current of the junctions.

To write down the Hamiltonian in a qubit representation we need to project it into the two-level subspaces with respect to the qubits. A standard way of doing this is to approximate the two wells of the flux-qubit potential as shifted harmonic oscillators [17] and interpret the two persistent current states of the qubit as the lowest eigenstates of these symmetrically shifted oscillators [18]. This leads to

$$\hat{\varphi}_j \approx s_j\hat{Z}_j, \quad (5)$$

where $\hat{Z}_j$ denotes the Pauli spin operator in the persistent-current basis. The factor $s_j \propto (1-\langle 0_+|0_-\rangle^2)^{-1/2}$ accounts for the fact that the two shifted ground states are not orthogonal, meaning that s_j would be unity if the overlap of these states were zero (see Appendix B for further details). Using this notation, we can write the interaction Hamiltonian as

$$\hat{H}_{\rm int} = E_{\tilde{L}_c}\left((\alpha s)^2\sum_{i,j=1}^{4}\hat{Z}_i\hat{Z}_j + \alpha s\sum_{i=1}^{4}\hat{Z}_i\hat{\varphi}_c\right), \quad (6)$$

where we assume identical qubits ($\alpha_i s_i = \alpha s$ for all i). The first part induces two-body local interactions between the qubits, which we call the direct-coupling part, and the second part describes the interaction between the qubits and the coupler modes, here referred to as indirect coupling. In commonly used coupler architectures, one chooses parameters such that the direct coupling dominates and the two local interactions become strong. Here we want to use a different strategy, where we choose parameters such that the direct-interaction part is rather small compared with the indirect-coupling part, which gives rise to two but also higher-order local interactions.

To see how these higher-order local interactions are indicated by the indirect-interaction part, we use a prominent tool from many-body physics, the Schrieffer-Wolff transformation (SWT) [19,20]. We choose the SWT since it produces physically transparent analytical expressions for the induced interactions arising from the indirect-coupling part of Eq. (6). Other than the simplest form of the Born-Oppenheimer approximation [21], it does not rely on the separation of classical frequencies and effective potentials. It is thus applicable even if transitions are vertical in the coordinate and if in the deep nonlinear regime classical frequencies are ill-defined (worse results for symmetric coupler potential in Ref. [22]). The SWT assumes that there are no transitions between different coupler levels, but includes corrections of the low-energy subspace due to the existence of higher levels. Hence, with the SWT it is possible to perturbatively write down an effective Hamiltonian in this low-energy subspace:

$$\hat{H}_{\rm eff} = \hat{P}_0\hat{H}_0\hat{P}_0 + \epsilon\hat{P}_0\hat{V}\hat{P}_0 + \sum_{n=2}^{\infty}\epsilon^n\hat{H}_{{\rm eff},n}, \quad (7)$$

where $\hat{H}_0 = \hat{H}_c + \sum_j\hat{H}_j$ is the unperturbed Hamiltonian, $\hat{V} = \hat{H}_{\rm int}$ is the perturbation, here the interaction, $\epsilon = \alpha s$ is a small parameter, and $\hat{P}_0$ projects the Hamiltonian into the low-energy subspace (coupler ground state). Every order of the effective Hamiltonian leads to higher-order local interactions between the qubits; that is, in general, the kth perturbative term contains induced interactions up to kth order. Truncation at fourth order therefore includes fourth-order local interactions, such that the effective Hamiltonian has the form

$$\hat{H} \approx \hat{P}_0\hat{H}_0\hat{P}_0 + J_2\sum_{i<j}\hat{Z}_i\hat{Z}_j + J_4\hat{Z}_1\hat{Z}_2\hat{Z}_3\hat{Z}_4. \quad (8)$$

The coupling strengths J_j are given by the prefactors generated by the SWT. J_2 additionally includes direct interactions arising from the second term in Eq. (7). In general, the Schrieffer-Wolff expansion also gives rise to single $\hat{Z}$ rotations and three-body terms, but since we choose a symmetric coupler potential these terms are negligible, as we argue in the following.

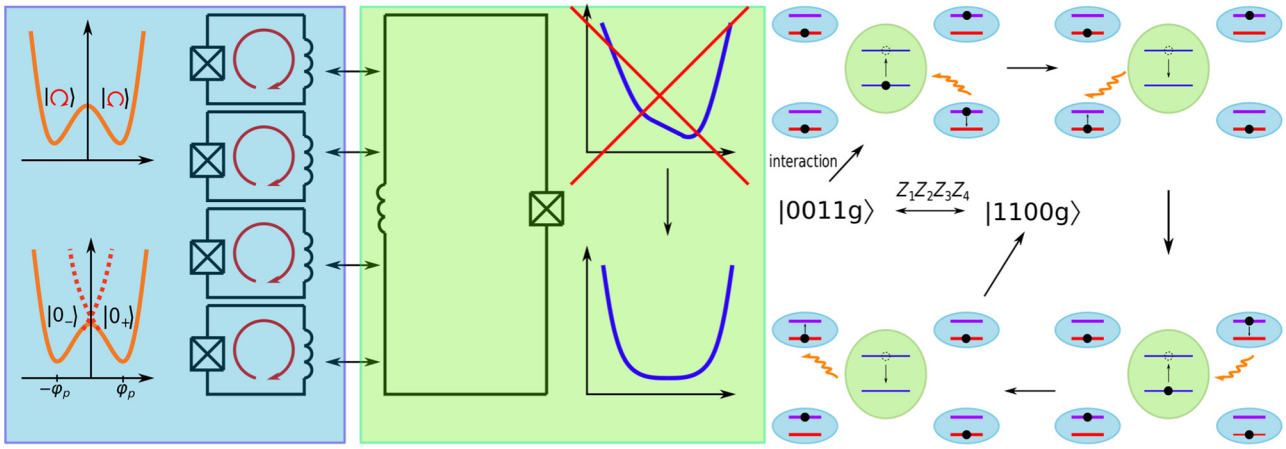

FIG. 1. Left: Setup of the coupler architecture. Four flux qubits are inductively coupled to an additional flux qubit with higher energy via mutual inductances M_j. We see the qubit double well potential, which can be approximated by two shifted harmonic potentials with eigenstates $|0_-\rangle$ and $|0_+\rangle$ corresponding to the persistent current states $|\circlearrowleft\rangle$ and $|\circlearrowright\rangle$ of the qubits. We choose a symmetric coupler potential to reduce $\hat{Z}$ corrections arising from $\hat{H}_{\text{int}}$ by biasing the coupler at the flux degeneracy point, as shown on the right of the coupler. Right: Visualization of four local interactions induced by virtual coupler transitions. A virtual excitation and annihilation of the coupler leads to energy transfer between two qubits, and hence two such processes can induce effective four local interactions.

The physical principle behind these indirect interactions can be understood with the language of virtual excitations. For example, the second order describes de-excitation of an excited qubit resulting in a virtual excitation of the coupler, which de-excites again and in turn excites the same or another qubit. Such processes leave the coupler in the ground state, but result in higher-order qubit interactions. These virtual processes can be thought to occur only within the Heisenberg energy-time uncertainty. Fourth-order processes in the same manner lead to four local interactions as illustrated in Fig. 1. For the first and third orders, there are no such processes, and the coupler ends up in the ground state; hence, they can be ignored in Eq. (8) (2–3 orders of magnitude smaller as can be seen from the Hamiltonian and Appendix C).

III. RESULTS

A. Numerical results

Since our qubit modeling using Eq. (5) is not very accurate for qubit nonlinearities only slightly larger than unity, we solve the system numerically and study the resulting spectrum. Here we evolve the bare-qubit and coupler Hamiltonian in harmonic oscillator modes using about 50 oscillator states, and then project the interaction parts into the low-energy subspace and determine the resulting spectrum numerically. The corresponding coupling strengths can be extracted from the spectrum by the distance of certain energy levels. In more detail we look at the two-excitation subspace of the spectrum, which is enlarged on the right of Fig. 2. Within this subspace, the distance between the different lines at the point where all frequencies are equal ($\omega_{1/2}/\omega_{2/3} = 1$) can be calculated analytically. These distances depend on J_2 and J_4; hence, it is possible to translate the resulting spectrum into coupling strengths.

The results for a device with realizable qubit and coupler parameters are shown in Fig. 2. All the contributions from the indirect-coupling term increase with the coupler nonlinearity β_c. We see that for $\beta_c \approx 0$ the two local interactions are dominated by the antiferromagnetic direct-coupling part and with increasing nonlinearity become more and more dominated by the ferromagnetic contribution from the indirect part. This results in a change in the nature of the interactions from antiferromagnetic to ferromagnetic at $\beta_c \approx 0.2$. The four local interactions, on the other hand, are antiferromagnetic for all nonlinearities, since they arise only from the indirect coupling. Also we observe that J_2 and J_4 have a crossing point at $\beta_c \approx 0.05$. For higher nonlinearites $|J_4|$ is larger than $|J_2|$. Both coupling strengths increase with increasing β_c, but for the parameters chosen at β_c around 0.7 the energy levels of the coupler ground-state subspace and coupler excited-state subspace start to mix, such that we can no longer use the setup to mimic the spectrum of the general Ising Hamiltonian including four local interactions. This is the reason why the results in Fig. 2 are restricted to $\beta_c < 0.7$ (see Appendix E).

A well-distinguishable point in the spectrum is $J_4 = -2J_2$. In the two-excitation subspace of the generalized four-qubit Ising Hamiltonian including fourth-order interactions, one observes three different energy levels, a nondegenerate one, a twice-degenerate one, and a 3-times-degenerate one. At the specific point $J_4 = -2J_2$, this behavior changes and only two different energies are left over, a twice-degenerate one and a 3-times-degenerate

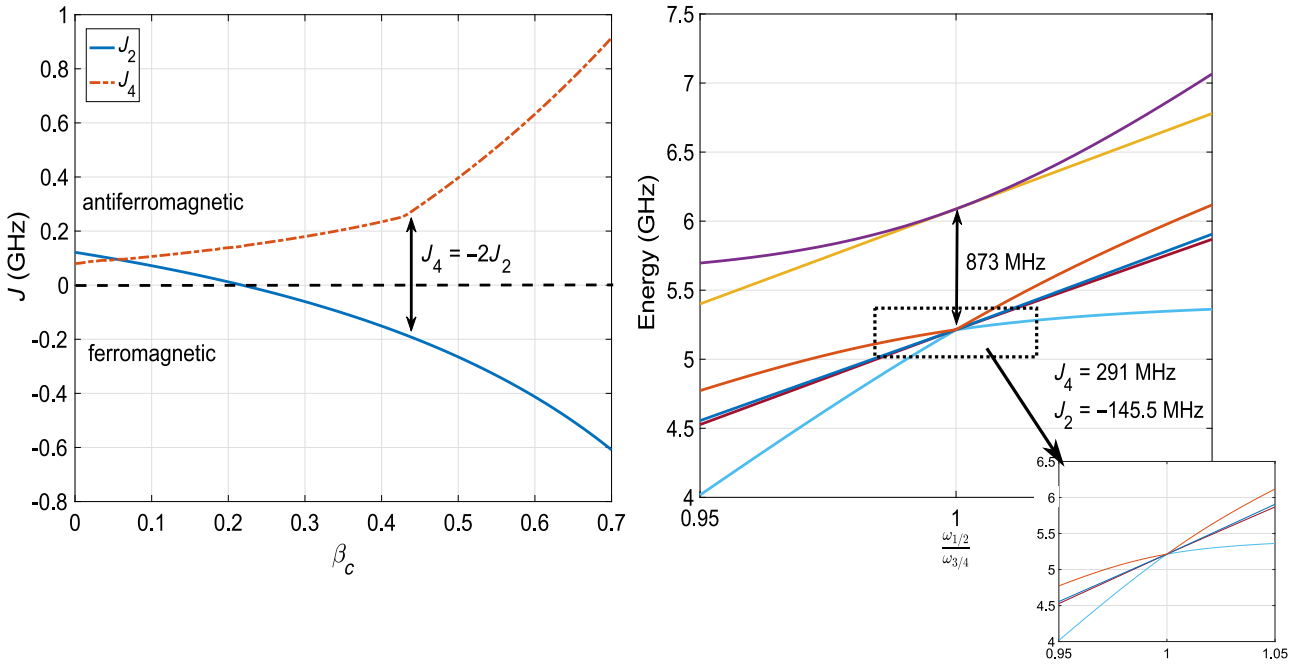

FIG. 2. Left: Coupling strength depending on the nonlinearity of the coupler for $E_{\tilde{L}_c} = 1$ THz, $\xi_c = 0.01$, $\xi_j = 0.05$, $\alpha_j = 0.05$, and $\beta_j = 1.1$. This corresponds to the physical qubit and coupler parameters $L_j = 817$ pH and $C_j = 77$ fF and $L_c = 170$ pH and $C_c = 407$ fF, respectively, with mutual inductance $M = 40$ pH. Right: Numerically determined spectrum of the two-excitation subspace for $E_j/E_{\tilde{L}_c} = 0.2$. One sees exactly the spectrum theoretically expected at this specific point, and the corresponding coupling strengths are $J_4 = 291$ MHz and $J_2 = -145.5$ GHz. The x axis denotes the ratio between the frequency of qubit 1 and 2 and qubit 3 and 4, where we choose ω_1 and ω_2 to be constant and vary the frequency of the third and fourth qubits at the same time but equally.

one. Our results indicate that this point is at $\beta_c = 0.43$; the numerically calculated spectrum for this specific nonlinearity is shown in Fig. 2 (right). We see exactly the theoretically expected behavior of the spectrum. For equal qubit frequencies the spectrum shows only two different energy levels, one that is twice degenerate and one that is 4 times degenerate. The distance between these two energy levels is $3J_4$. For the parameters chosen and a realistic $E_{\tilde{L}_c}$ of about 1 THz, we observe coupling strengths of $J_4 = 291$ MHz and $J_2 = -145.5$ MHz. By increasing β_c, one can tune the four-body interactions close to the gigahertz range. This is the largest predicted strength of four local interactions in a superconducting qubit architecture without ancilla qubits. The coupling could also be made to be tunable by use of a flux-qubit architecture with tunable nonlinearity [e.g., a tunable rf superconducing quantum-interference device (SQUID) [23] instead of the rf-SQUID coupler]. For the sense of completeness, we acknowledge that there is a proposal for a four-body flux-qubit coupler with comparable coupling strengths by Kerman [24]. In contrast to our setup, Kerman uses a more-complicated coupler setup, combining two devices, to realize the four local interactions, but therefore Kerman are able to get rid of the two local interactions. Additionally there also is recent a proposal by Melanson *et al.* [25] to realize three local interactions using an additional twisted coupler

B. Analytical results

To get analytical results we calculate the SWT up to fourth order. This can be done in two different ways, the fully analytical way, where we truncate the cosine of the coupler potential after fourth order, and the numerical way, where we keep the full cosine and need to calculate the respective coupling strengths resulting from the SWT numerically. In both cases the qubit potentials are approximated by two shifted harmonic oscillators as explained in the previous section and in more detail in Appendix B. Especially the fully analytical approach leads to the calculation of nasty commutators and long expressions for the coupling strengths. Therefore, the full calculations can be found in Appendix C, and we only discuss the results here.

Although the calculated results qualitatively give the right behavior of the different coupling strengths, the actual values found analytically differ from the numerical ones. As mentioned before, the reason is the rather-small barrier of the qubit potential, making the validity of the shifted-harmonic-oscillator approximation we used to model the qubits not reliable. This leads to a wrong prefactor s_j [see Eq. (5)] arising from the analytical qubit-subspace projection. Also the larger β_c gets, the more-important higher orders of the SWT become. In Fig. 3 we show the results for the fully analytical SWT and for the numerical SWT. We see that they show the right qualitative behavior and

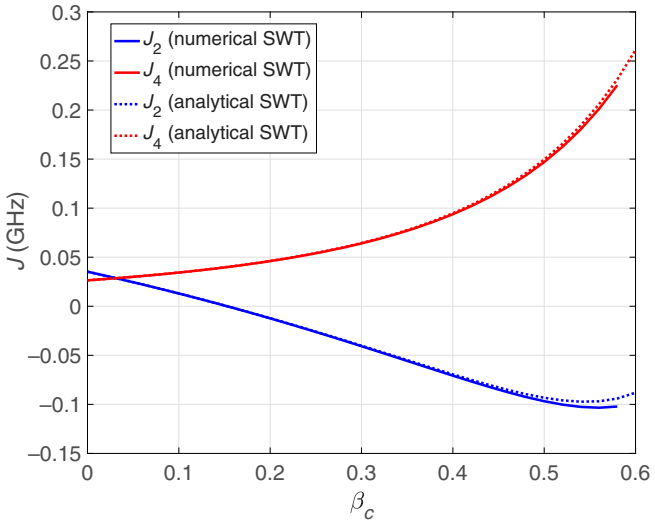

FIG. 3. Comparison between the coupling strengths for the fully analyical SWT and the numerical SWT for the same parameters as in Fig. 2.

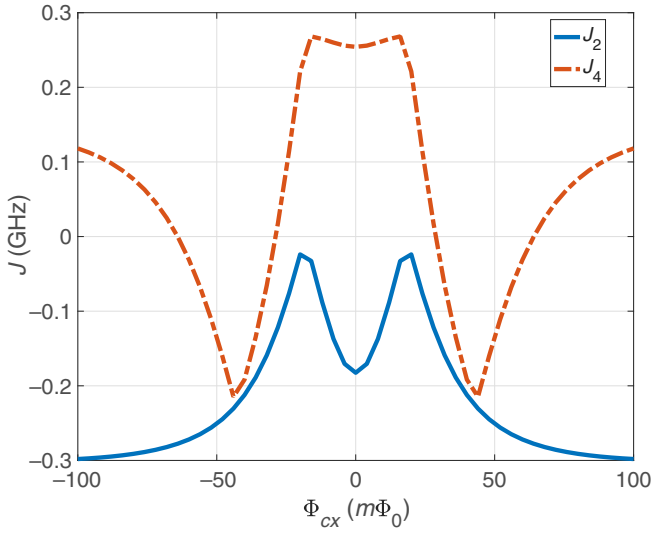

FIG. 4. Variation of the coupling strengths for a small external flux applied to the coupler loop. System parameters are the same as in Fig. 2.

order of magnitude of the coupling strengths, but the actual values differ from the ones found via numerical simulation. For example, for the specific point $\beta_c = 0.43$ chosen in Fig. 2, analytically calculated results predict $J_4 = \approx 112$ MHz and $J_2 \approx -80$ MHz. Another thing we see is that for $\beta_c \approx 0.55$ the two-body coupling seems to have a minimum and then changes slope. This can be explained by the fact that larger β_c leads to a smaller gap and at some point higher orders of the SWT are important. This means that we would not see this minimum but rather the behavior found in the numerical simulations when we start adding higher orders. Also higher orders of the coupler's cosine-potential part have more and more influence for higher β_c, explaining the slight differences between the two analytical approaches (fully analytic SWT and numerical SWT) for large β_c.

IV. FLUX-NOISE EFFECTS

So far we have assumed a perfect coupler with four identical qubits and no external noise. However, in real flux-qubit experiments a crucial effect is flux noise, which is present in all superconducting circuits. In Hamiltonians (2) and (3) flux noise can be described as an additional external flux Φ_{jx} on the qubit and coupler loops, respectively. An external flux on the qubit loops induces a small tilt of the double-well potential driving it slightly away from the flux degeneracy point. However, this effect just adds a small $\hat{Z}_j$ contribution to the qubit Hamiltonians. The most-important influence of flux noise is the external noise applied to the coupler loop. This can significantly change the respective coupling strengths. In Fig. 4 we show J_2 and J_4 under the influence of an external current on the coupler loop. We see that small flux variations do not change the four-local-interaction strength, indicating a magic point for flux noise at $\Phi_{cx} = \Phi_0/2$. Such a point arises when first-order corrections of flux fluctuations vanish due to symmetry properties [26] when the first-order dephasing rate induced by the environment (Fermi's golden rule contribution) vanishes. Only the two local interactions are affected. However, the two local interactions become smaller, meaning we can apply an external flux to discriminate the two local interactions, leading to J_4 in the gigahertz range and J_2 about 2 orders of magnitude smaller. Driving the system slightly away from the degeneracy point also adds linear $\hat{Z}_j$ corrections to the qubits. However, for the parameters chosen, the $\hat{Z}_j$ corrections can be estimated from the Hamiltonian to be approximately 10 GHz per flux quantum, which results in $J_1 \approx 3$ MHz for the sweet spot shown in Fig. 4. The flux-offset range in Fig. 4 is chosen to be orders of magnitude larger than typical flux offsets to visualize the appearance of the plateau in the four local interactions.

The range of flux offset shown in Fig. 4 is well above flux offsets that are induced by typical noise sources, and it is chosen such that the appearance of a magic point is more visible. The noise that is most present in superconducting flux-qubit architectures is $1/f$ flux noise, which gets its name from the respective power spectral density being proportional to the reciprocal frequency [27]. However, typical flux-noise amplitudes are around 1–10 $\mu\Phi_0$ [28], meaning the induced flux offsets are also in this range. Since the whole circuit presented here would be built on one chip, meaning it is surrounded by the same electrical environment, we assume a constant flux offset at both the coupler and all four qubits. Figure 5 shows the dependence of the coupling strength on the flux offset

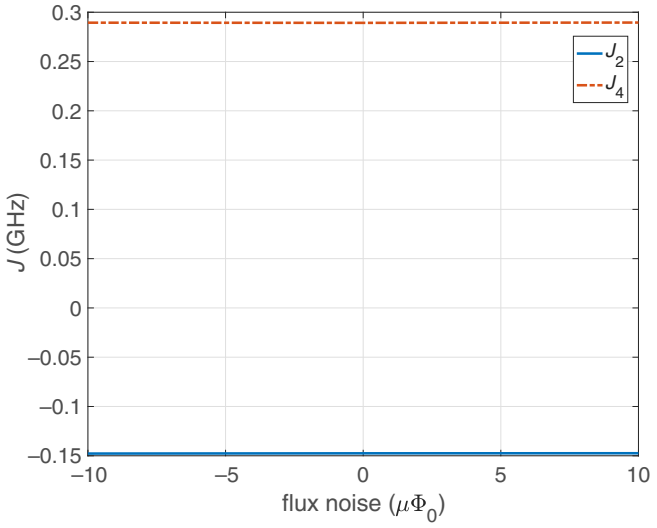

FIG. 5. Dependence of coupling strength of our setup on the flux offset induced in the coupler and all four qubits.

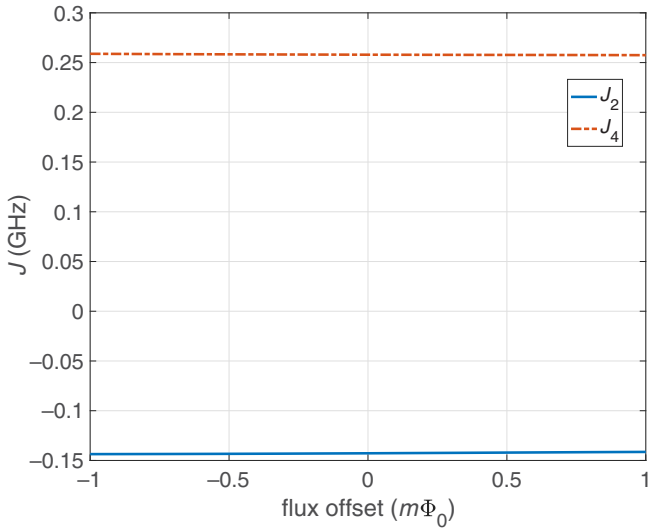

FIG. 6. Dependence of the coupling strength of our setup on the flux offset in the coupler with additional fixed flux offsets on the qubits: $\Phi_{c,1} = 1\ \mathrm{m}\Phi_0$, $\Phi_{c,2} = 1.5\ \mathrm{m}\Phi_0$, $\Phi_{c,3} = -2.1\ \mathrm{m}\Phi_0$, and $\Phi_{c,4} = 3\ \mathrm{m}\Phi_0$.

induced in the coupler and all four qubits. We see that for typical noise amplitudes the change in coupling strength is not significant, meaning that the circuit is very robust against the usual flux noise occurring in superconducting architectures.

Another effect that is important to study is the effect of flux offsets in the controls, meaning different flux offsets acting on the four qubits. This leads to the four qubits being at four different bias points, and symmetry effects such as the plateau seen in Fig. 4 may no longer be present. In real experiments there are two reasons for such flux offsets: on the one hand, flux $1/f$ noise which leads to long-term drifts because of nonvanishing expectation values (the value is obtained from the integrated power spectral density, and standard values are between 10 and 100 $\mu\Phi_0$); on the other hand, such control offsets can be caused by resolution itself. With arbitrary-waveform generators and a resolution of at least ten bits with a range split over a couple of flux quanta, this leads to a rather high offset of about 1 $\mathrm{m}\Phi_0$. To prove that these effects do not affect our system dramatically, we choose four random flux offsets in the milli-flux-quantum range and study the variation of the coupling strengths with variation of the coupler flux offset in the same range. The result is shown in Fig. 6, and we again see that for typical values found in experiments the effect on the coupling strength is not crucial. The overall value is slightly changed, but it stays constant over the whole range of coupler offsets, meaning it is not more susceptible to noise away from the symmetric bias case.

Another effect that appears in real experiments, especially when using artificial atoms as qubits are fabrication errors leading to uncertainties in the system parameters. This is studied in detail in Appendix F and we show that our setup is rather robust against these.

V. CONCLUSION

In conclusion, we show that the coupling architecture presented in Fig. 1 can exhibit large effective four-body local interactions in the deep nonlinear regime. With suitable realistic parameters, they are even larger than the two-body local interactions and are in the gigahertz range. To our knowledge these are (together with Ref. [24]) the strongest four-body local interactions ever predicted in an architecture without additional ancilla qubits. Building such a device could yield a strong improvement of the applicability of quantum annealers. Also it would be possible to use a slightly different qubit arrangement or a twist in the coupler (comparable to Ref. [25]) to change the sign of the two and four local interactions to directly implement ferromagnetic four-body interactions, which are often desired [29]. Such an additional coupler could also be used to completely get rid of the two local interactions as reported in Ref. [25], leading to a bare four-body coupler.

The architecture presented could be used to build more-efficient adiabatic quantum computers on the platform of superconducting flux qubits and exhibit the limits of currently used architectures (e.g., D-Wave). Furthermore, as discussed at in Sec. I, the realization of a four-body coupler could be the next step toward the quantum technological implementation of a universal AQC.

ACKNOWLEDGMENTS

We thank Adrian Lupaşcu, Denis Melanson, Andrew J. Kerman, and Simon Jäger for fruitful discussions that increased the quality of this work.

The research is based on work (partially) supported by the Office of the Director of National Intelligence (ODNI), Intelligence Advanced Research Projects Activity (IARPA), via U.S. Army Research Office Contract No. W911NF-17-C-0050. The views and conclusions contained herein are those of the authors and should not be interpreted as necessarily representing the official policies or endorsements, either expressed or implied, of the ODNI, IARPA, or U.S. Government. The U.S. Government is authorized to reproduce and distribute reprints for Governmental purposes notwithstanding any copyright annotation thereon.

APPENDIX A: CIRCUIT HAMILTONIAN

Here we show how to get from Kirchhoff's laws to the Hamiltonian (A8) of the circuit shown in Fig. 1 using circuit quantization. The section mostly recaps calculations that can be found in Ref. [22], but for completeness we also show them here. In our setup we inductively couple four superconducting flux qubits using a coupling loop, realized by an additional flux qubit with higher plasma frequency than the four qubits. Kirchhoff's laws and Josephson's equations give the current equations of the system:

$$C\ddot{\Phi}_c + I_c^{(c)} \sin(2\pi\Phi_c/\Phi_0) - I_{L,c} = 0, \tag{A1}$$

$$I_j - I_j^* = 0 \quad (1 \le j \le k). \tag{A2}$$

For the first equation, Φ_c denotes the flux across the coupler's Josephson junction (and capacitor), $I_{L,c}$ denotes the current through the coupler's inductor, and $\Phi_0 = h/(2e)$ is the flux quantum. The second equation simply states that the current I_j through the jth inductor is equal to the current I_j^* flowing through the rest of the qubit circuit. We leave the factors I_j^* like this since we will see that they do not contribute to the interaction part and later lead to the usual flux-qubit Hamiltonian [16]. The inductive and flux quantization relationships can be combined into

$$L_c I_{L,c} + \sum_{j=1}^{k} M_j I_j = \Phi_{L,c}, \tag{A3}$$

$$L_j I_j + M_j I_{L,c} = \Phi_j, \tag{A4}$$

$$\Phi_{L,c} = \Phi_{cx} - \Phi_c, \tag{A5}$$

where Φ_{cx} is the external flux applied to the coupler loop, Φ_j is the flux across the jth junction, L_j is the jth-qubit self-inductance, and M_j is the mutual inductance between the jth qubit and the coupler. With Eqs. (A3)–(A5) it is possible to rewrite Eqs. (A1) and (A2) in flux variables,

$$C\ddot{\Phi}_c I_c^{(c)} \sin(2\pi\Phi_c/\phi_0) + \frac{\Phi_c - \Phi_{cx} + \sum_{i=j}^{4} \alpha_i \Phi_j}{\tilde{L}_c} = 0, \tag{A6}$$

$$\frac{\Phi_j}{L_j} + \alpha_j \left(\Phi_c - \Phi_{cx} + \sum_{k=1}^{4} \alpha_k \Phi_k \right) - I_j^* = 0, \tag{A7}$$

with dimensionless mutual inductance $\alpha_j = M_j/L_j$ and rescaled coupler impedance $\tilde{L}_c = L_c - \sum_{j=1}^{4} \alpha_j M_j$. These equations of motion represent the Euler-Lagrange equation, resulting from the Lagrange function of the system. Now one can apply circuit quantization to find the corresponding Hamiltonian. From Eqs. (A6) and (A7) we know the Lagrangian, which can be used to define the adjoint variable to the flux and write down a quantized version of the system Hamiltonian using the Legendre transformation. This leads to the Hamiltonian

$$\hat{H} = \frac{\hat{Q}^2}{2C} - E_{J_c} \cos(2\pi\hat{\Phi}_c/\Phi_0) + \frac{\left(\hat{\Phi}_c - \Phi_{cx} + \sum_{j=1}^{k} \alpha_j \hat{\Phi}_j\right)^2}{2\tilde{L}_c} + \sum_{j=1}^{k} \hat{H}_j, \tag{A8}$$

where $\hat{H}_j$ denotes the Hamiltonian for qubit j in the absence of the coupler (i.e., in the limit $\alpha_j \longrightarrow 0$), $\hat{Q}_c$ is the canonical conjugate to $\hat{\Phi}_c$ satisfying $\left[\hat{\Phi}_c, \hat{Q}_c\right] = i\hbar$, and the coupler's Josephson energy $E_{J_c} = \Phi_0 I_c^{(c)}/2\pi$.

The Hamiltonian can be rewritten in unitless parameters:

$$\hat{H} = E_{\tilde{L}_c} \left(4\zeta_c^2 \frac{\hat{q}_v^2}{2} + \frac{(\hat{\varphi}_c - \varphi_x)^2}{2} + \beta_c \cos\hat{\varphi}_c \right) + \sum_{i=1}^{4} \hat{H}_j, \tag{A9}$$

$$\hat{H}_j = E_{\tilde{L}_j} \left(4\zeta_j^2 \frac{\hat{q}_j^2}{2} + \frac{(\hat{\varphi}_j - \varphi_x)^2}{2} + \beta_j \cos\hat{\varphi}_j \right), \tag{A10}$$

where

$$E_{\tilde{L}_c} = \frac{(\Phi_0/2\pi)^2}{\tilde{L}_c}, \quad \xi_c = \frac{2\pi e}{\Phi_0}\sqrt{\frac{\tilde{L}_c}{C}}$$

$$\beta_c = 2\pi\tilde{L}_c I_c^{(c)}/\Phi_0 = E_{J_c}/E_{\tilde{L}_c}, \quad \hat{q}_c = \frac{\hat{Q}}{2e}$$

$$\hat{\varphi}_c = \frac{2\pi}{\Phi_0}\hat{\Phi}_c + \pi, \quad \varphi_{cx} = \frac{2\pi}{\Phi_0}\Phi_{cx} + \pi$$

$$\hat{\varphi}_j = \frac{2\pi}{\Phi_0}\hat{\Phi}_j, \quad \hat{\varphi}_x = \varphi_{cx} - \sum_{j=1}^{k} \alpha_j \hat{\varphi}_j.$$

The phases $\hat{\varphi}$ are shifted by a factor π such that the flux degeneracy point corresponds to $\varphi_{cx} = 0$.

APPENDIX B: PROJECTION INTO QUBIT SUBSPACE

Since we are interested in qubit interactions, we want to project the qubit part of the Hamiltonian into the subspace of the two lowest eigenstates of every included qubit (computational states). To do so, we consider the qubit potential:

$$U_j(\varphi_j) = \frac{1+\alpha_j^2}{2}\varphi_j^2 + \beta_j \cos\varphi_j . \tag{B1}$$

In case of a flux qubit, the nonlinearity β_j should be larger than 1. This leads to a double-well potential. The local maximum is located at $\varphi = 0$ and the two symmetric minima are located at $\varphi = \pm\varphi_p$. Now we approximate the two wells of the potential with two harmonic potentials, shifted by $\pm\varphi_p$, respectively . The equation that determines φ_p reads

$$0 = (1+\alpha_j)\varphi - \beta_c \sin\varphi_p, \tag{B2}$$

which can easily be solved numerically. To get a harmonic approximation, we evolve the respective potential well around $\pm\varphi_p$ up to second order:

$$U^+(\varphi) = c + U'(\varphi_p)(\varphi-\varphi_p) + U''(\varphi_p)(\varphi-\varphi_p)^2, \tag{B3}$$

$$U^-(\varphi) = c + U'(-\varphi_p)(\varphi+\varphi_p) + U''(-\varphi_p)(\varphi+\varphi_p)^2. \tag{B4}$$

The constant part can be ignored, and the first derivative vanishes, since φ_p satisfies Eq. (B2). Hence, we get

$$\begin{aligned} U(\varphi) &\approx U^+(\varphi) + U^-(\varphi) \\ &= \frac{1+\alpha_j-\beta_j\cos\varphi_p}{2}(\varphi-\varphi_p)^2 \\ &\quad + \frac{1+\alpha_j-\beta_j\cos\varphi_p}{2}(\varphi+\varphi_p)^2. \end{aligned} \tag{B5}$$

To quantize the system we introduce the raising and lowering operators of the two shifted quadratic potentials:

$$\hat{a}_\pm^\dagger |N_\pm\rangle = \sqrt{N_\pm+1}\,|N_\pm+1\rangle , \tag{B6}$$

$$\hat{a}_\pm |N_\pm\rangle = \sqrt{N_\pm}\,|N_\pm-1\rangle , \tag{B7}$$

where $|N_\pm\rangle$ are the Fock states of the respective shifted harmonic oscillator. For more details on the displaced-harmonic-oscillator basis, see Ref. [17]. We want to restrict the basis to the two lowest energy levels (qubit basis). In the flux basis, they are the superpositions of the ground states $|0_\pm\rangle$ of the two wells:

$$|\tilde{0}\rangle = \frac{1}{\sqrt{2}}\left(|0_+\rangle + |0_-\rangle\right), \tag{B8}$$

$$|\tilde{1}\rangle = \frac{1}{\sqrt{2}}\left(|0_+\rangle - |0_-\rangle\right). \tag{B9}$$

Here the two ground states $|0_\pm\rangle$ correspond to the persistent-current states of the respective flux qubit. The two states are orthogonal, but since $\langle 0_+|0_-\rangle \neq 0$, we need to redefine an orthonormal qubit basis:

$$|0\rangle = \frac{1}{\sqrt{2(1+\langle 0_+|0_-\rangle)}}\left(|0_+\rangle + |0_-\rangle\right), \tag{B10}$$

$$|1\rangle = \frac{1}{\sqrt{2(1-\langle 0_+|0_-\rangle)}}\left(|0_+\rangle - |0_-\rangle\right). \tag{B11}$$

Using all the properties, we write down in this section, we can translate the quantized phase into an operator acting only in the new defined qubit subspace:

$$\hat{\varphi}_j \longmapsto \frac{1}{\sqrt{2m_j\omega_j(1-\langle 0_-|0_+\rangle^2)}}\hat{X}_j, \tag{B12}$$

where $m_j = 1/4\xi_j^2$ and $\omega_j = 2\xi_j\sqrt{1+\alpha_j^2-\beta_c\cos\varphi_p}$ are the effective mass and frequency of the quadratic potential and $\hat{X}_j$ is the Pauli spin operator in the qubit basis. For simplification, we additionally define the factor

$$s_j = \frac{1}{\sqrt{2m_j\omega_j(1-\langle 0_-|0_+\rangle^2)}},$$

which also appears in the main text. The overlap between the states in the displaced wells can be calculated by the formula [17]

$$\langle M_-|N_+\rangle = \begin{cases} e^{-\varphi_p^2/2}(-\varphi_p)^{M-N}\sqrt{N!/M!}L_N^{M-N}[\varphi_p^2], & M \geq N, \\ e^{-\varphi_p^2/2}(-\varphi_p)^{N-M}\sqrt{M!/N!}L_M^{N-M}[\varphi_p^2], & M < N, \end{cases} \tag{B13}$$

where L_n^k are the generalized Laguerre polynomials. In the flux-qubit literature it is more common to write down the Hamiltonian in the persistent-current basis rather than the qubit basis; hence, the flux is proportional to Z_j instead of X_j ($X_j \mapsto Z_j$) in the following and in the main text.

APPENDIX C: ANALYTICAL APPROXIMATION OF THE EFFECTIVE SCHRIEFFER-WOLFF HAMILTONIAN

Here we show how to get an analytical approximation for the SWT by expressing the harmonic part of the coupler using latter operators and treating the cosine part as a perturbation. For this we truncate the coupler potential after $\mathcal{O}(\hat{\varphi}_c^4)$. The interaction part of the Hamiltonian then reads

$$\hat{H}_{\rm int}/E_{\tilde{L}_c} = \frac{\beta_c}{24}\hat{\varphi}_c^4 + \alpha^2 \sum_{i<j}^{4} \hat{\varphi}_i\hat{\varphi}_j - 2\varphi_{cx}\hat{\varphi}_c + \alpha \sum_{i=1}^{4} \hat{\varphi}_c\hat{\varphi}_i + \varphi_{cx}\sum_{i=1}^{4}\hat{\varphi}_i. \tag{C1}$$

For simplicity we chose identical qubits here. Now we assume a symmetric coupler potential $\varphi_{cx} = 0$ and use Eq. (B12) to project the Hamiltonian into the qubit subspace:

$$\hat{H}_{\rm int}/E_{\tilde{L}_c} = \frac{\beta_c}{24}\hat{\varphi}_c^4 + \alpha^2 s^2 \sum_{i<j}^{4} \hat{Z}_i\hat{Z}_j + \alpha s \sum_{i=1}^{4} \hat{\varphi}_c\hat{Z}_i. \tag{C2}$$

The harmonic part of the coupler potential

$$\hat{H}_c^{\rm harm} = 4E_{\tilde{L}_c}\left(\xi_c^2\frac{\hat{q}_c^2}{2} + \frac{1-\beta_c}{2}\hat{\varphi}_c^2\right) \tag{C3}$$

can be interpreted as a quantum harmonic oscillator with effective mass $m_c = 1/4E_{\tilde{L}_c}\xi_c^2$ and frequency $\omega_c = 2E_{\tilde{L}_c}\xi_c\sqrt{1-\beta_c}$. The coupler nonlinearity β_c is assumed to be smaller than 1 since we want the coupler frequency to be higher than the qubit frequencies. With this we can define the position operator and momentum operator as

$$\hat{X}_c = \sqrt{m_c\omega_c}\hat{\varphi}_c, \tag{C4}$$

$$\hat{P}_c = \frac{1}{\sqrt{m_c\omega_c}}\hat{q}_c, \tag{C5}$$

and we can rewrite the harmonic part as $\hat{H}_c^{\rm harm} = \frac{\omega_c}{2}(\hat{X}_c^2 + \hat{P}_c^2)$. In the same manner we can define the annihilation operator and creation operator as

$$\hat{a}_c = \frac{1}{\sqrt{2}}\left(\hat{X}_c + i\hat{P}_c\right), \tag{C6}$$

$$\hat{a}_c^\dagger = \frac{1}{\sqrt{2}}\left(\hat{X}_c - i\hat{P}_c\right), \tag{C7}$$

and we can rewrite the quantized phase in terms of these operators:

$$\hat{\varphi}_c = \frac{1}{\sqrt{2m_c\omega_c}}\left(\hat{a}_c^\dagger + \hat{a}_c\right). \tag{C8}$$

Using Eq. (C8), we can rewrite the interaction Hamiltonian in terms of the latter operators:

$$\hat{H}_{\rm int}/E_{\tilde{L}_c} = \frac{\beta_c}{24}\frac{1}{(2m_c\omega_c)^2}\left(\hat{a}_c^\dagger + \hat{a}_c\right)^4 + \alpha^2 s^2 \sum_{i<j}^{4}\hat{Z}_i\hat{Z}_j + \alpha s\sum_{i=1}^{4}\frac{1}{\sqrt{2m_c\omega_c}}\left(\hat{a}_c^\dagger + \hat{a}_c\right)\hat{Z}_i. \tag{C9}$$

To get a better overview, we divide Eq. (C9) into three parts, the direct qubit-qubit coupling

$$\hat{H}_{\rm int}^{\rm QB,QB} = E_{\tilde{L}_c}\alpha^2 s^2 \sum_{i<j}\hat{Z}_i\hat{Z}_j, \tag{C10}$$

the indirect coupling between qubits and coupler modes

$$\hat{H}_{\rm int}^{\rm QB,c} = \frac{E_{\tilde{L}_c}}{\sqrt{2m_c\omega_c}}\alpha s\sum_{i=1}^{4}\left(\hat{a}_c^\dagger + \hat{a}_c\right)\hat{Z}_i, \tag{C11}$$

and the corrections arising from the fourth-order cosine part

$$\hat{H}_{\rm corr} = \frac{E_{\tilde{L}_c}\beta_c}{96m_c^2\omega_c^2}\left(\hat{a}_c^\dagger + \hat{a}_c\right)^4. \tag{C12}$$

To simplify the notation even more in the following, we define the prefactors that appear as follows:

$$g^{\rm QB,c} = \frac{E_{\tilde{L}_c}\alpha s}{\sqrt{m_c\omega_c}}, \tag{C13}$$

$$g^{\rm QB,QB} = E_{\tilde{L}_c}\alpha^2 s^2, \tag{C14}$$

$$K_{\rm corr} = \frac{E_{\tilde{L}_c\beta_c}}{96m_c^2\omega_c^2}. \tag{C15}$$

As mentioned in the main text, we want to perform the SWT under the assumption that the coupler frequency is higher than the respective qubit frequencies. Basically we have three different perturbative parts [Eqs. (C10), (C11), and (C12)], where $\hat{H}_{\rm int}^{\rm QB,QB}$ acts on just the qubit subspace, and hence simply gives a contribution of zeroth order.

In a first step we have to calculate the even and odd contributions of the perturbative parts. We define $P_0 = |0\rangle\langle 0|$ and $Q_0 = 1 - P_0 = \sum_{n=1}^{\infty}|n\rangle\langle n|$ as the projection operators on the even and odd subspaces, respectively. Here $|n\rangle$ denotes the nth Fock state of the harmonic coupler potential. The off-diagonal part of an operator $\hat{X}$ is then given by $\mathcal{O}(\hat{X}) = P_0\hat{X}Q_0 + Q_0\hat{X}P_0$ and the diagonal part is given by $\mathcal{D}(\hat{X}) = P_0\hat{X}P_0 + Q_0\hat{X}Q_0$. Since $\hat{H}_{\rm int}^{\rm QB,QB}$ acts as an

identity on the coupler subspace, it is completely diagonal. The other parts read

$$\mathcal{O}(\hat{a}^\dagger + \hat{a}) = \eta^+_{01}, \tag{C16}$$

$$\mathcal{O}((\hat{a}^\dagger + \hat{a})^4) = \sqrt{4!}\eta^+_{04} + 5\sqrt{2!}\eta^+_{02}, \tag{C17}$$

$$\mathcal{D}(\hat{a}^\dagger + \hat{a}) = \sum_{n=1}^{\infty} \eta^+_{n,n+1}, \tag{C18}$$

$$\mathcal{D}((\hat{a}^\dagger + \hat{a})^4) = \sum_{n=1}^{\infty} \left(A^{(4)}_n \eta^+_{n,n+4} + A^{(2)}_n \eta^+_{n,n+2} + A^{(0)}_n \frac{\eta^+_{n,n}}{2} \right), \tag{C19}$$

with $\eta^\pm_{k,l} = |k\rangle\langle l| \pm |l\rangle\langle k|$, $A^{(4)}_n = \sqrt{(n+4!/n!)}$, $A^{(2)}_n = \sqrt{n^2(n+1)(n+2)} + \sqrt{(n+1)^3(n+2)} + \sqrt{(n+1)(n+2)^3} + \sqrt{(n+1)(n+2)(n+3)^2}$, and $A^{(0)}_n = 6(n^2+n)$. Additionally, we calculate some useful commutators:

$$\left[\eta^+_{ij}, \eta^+_{kl}\right] = \delta_{jk}\eta^-_{il} + \delta_{jl}\eta^-_{ik} + \delta_{ik}\eta^-_{jl} + \delta_{il}\eta^-_{jk}, \tag{C20}$$

$$\left[\eta^-_{ij}, \eta^-_{kl}\right] = \delta_{jk}\eta^-_{il} - \delta_{jl}\eta^-_{ik} - \delta_{ik}\eta^-_{jl} + \delta_{il}\eta^-_{jk}, \tag{C21}$$

$$\left[\eta^-_{ij}, \eta^+_{kl}\right] = \delta_{jk}\eta^+_{il} + \delta_{jl}\eta^+_{ik} - \delta ik\eta^+_{jl} - \delta_{il}\eta^+_{jk}, \tag{C22}$$

$$\left[\eta^+_{ij}, \eta^-_{kl}\right] = \delta_{jk}\eta^+_{il} - \delta_{jl}\eta^+_{ik} + \delta ik\eta^+_{jl} - \delta_{il}\eta^+_{jk}. \tag{C23}$$

With this as a starting point we can calculate the different orders of the Schrieffer-Wolff corrections to the effective Hamiltonian. The zeroth order of the effective Hamiltonian is just the unperturbed part projected into the coupler ground-state subspace. The first-order corrections are given by the diagonal projections of the perturbation, so in our case only the part $\hat{H}^{\mathrm{QB,QB}}_{\mathrm{int}}$ and the diagonal parts arising from $\hat{H}_{\mathrm{corr}}$, which are zero because $A^0_n(0) = 0$. Hence, a real calculation is needed only for the corrections of order larger than 1. When calculated to a specific order, the SWT finally gives an effective Hamiltonian acting only on the subspace of interest (here the coupler in ground-state subspace), but including corrections coming from states not included in this subspace. The form of the effective Hamiltonian is given in Eq. (7). In the following we calculate the different orders of the SWT up to fourth order analytically.

1. Second-order effective Hamiltonian

First we calculate the first order of the generator S, which defines the SWT and is used to calculate the respective order of the effective Hamiltonian. The first order of S is given by

$$S_1 = \mathcal{L}(V_{\mathrm{od}}), \tag{C24}$$

where we use the notation of Bravyi *et al.* [20], such that V_{od} denotes all the off-diagonal parts of the perturbation Hamiltonian and the linear map $\mathcal{L}$ is defined as

$$\mathcal{L}(X) = \sum_{i,j} \frac{\langle i|\mathcal{O}(X)|j\rangle}{E_i - E_j} |i\rangle\langle j|, \tag{C25}$$

where $\{|i\rangle\}$ is an orthonormal eigenbasis of the unperturbed Hamiltonian. With this definition we can write down the expression for S_1:

$$S_1 = \sum_{i,j} \frac{\langle i|V^{\mathrm{QB},c}_{\mathrm{od}}|j\rangle}{E_i - E_j} |i\rangle\langle j| + \sum_{i,j} \frac{\langle i|V^{\mathrm{corr}}_{\mathrm{od}}|j\rangle}{E_i - E_j} |i\rangle\langle j|. \tag{C26}$$

In our case the $|i\rangle$'s are the eigenstates of the bare-coupler Hamiltonian (harmonic oscillator part). We need the following expressions to get S_1:

$$\langle i|\eta^+_{kl}|j\rangle = \delta_{ik}\delta_{jl} + \delta_{il}\delta_{kj} \tag{C27}$$

$$\Rightarrow \langle i|\eta^+_{10}|j\rangle = \frac{1}{E_1 - E_0}\eta^-_{10} \tag{C28}$$

$$\Rightarrow \langle i|\eta^+_{40} + \eta^+_{20}|j\rangle = \frac{1}{E_4 - E_0}\eta^-_{40} + \frac{1}{E_2 - E_0}\eta^-_{20}, \tag{C29}$$

such that we get

$$\begin{aligned} S_1 &= \sum_{j=1}^{4} \frac{g^{\mathrm{QB},c}_j \hat{Z}_j}{E_1 - E_0}\eta^-_{10} + K_{\mathrm{corr}} \left(\frac{\sqrt{4!}}{E_4 - E_0} + \frac{5\sqrt{2!}}{E_2 - E_0}\eta^-_{20} \right) \\ &= \sum_{j=1}^{4} \gamma^{(1)}_j \hat{Z}_j \eta^-_{10} + \beta^{(1)}_1 \eta^-_{40} + \beta^{(1)}_2, \end{aligned} \tag{C30}$$

where $\gamma^{(1)}_j = g^{\mathrm{QB},c}_j/(E_1 - E_0)$, $\beta^{(1)}_1 = \sqrt{4!}K_{\mathrm{corr}}/(E_4 - E_0)$, and $\beta^{(2)}_2 = 6\sqrt{2}K_{\mathrm{corr}}/(E_2 - E_0)$.

The second order of the effective Hamiltonian is then given by

$$H_{\mathrm{eff},2} = b_1 P_0 \hat{S}_1(V_{\mathrm{od}}) P_0, \tag{C31}$$

where we again adopt the notation of Barvyi *et al.* such that $\hat{S}_1(V_{\mathrm{od}}) = [S_1, V_{\mathrm{od}}]$. The prefactor b_1 is characterized by the equation

$$b_{2n-1} = \frac{2(2^{2n} - 1)B_{2n}}{(2n)!}, \tag{C32}$$

with Bernoulli numbers B_n. Using the commutation relations (C20)–(C23) and the fact that P_0 projects into the coupler ground-state subspace—only terms proportional to

η_{00} contribute—we get

$$\hat{H}_{\text{eff},2} = -\left(\sum_{i,j=1}^{4} \alpha_i^{(1)} g_j^{\text{QB},c} \hat{Z}_i \hat{Z}_j + \beta_1^{(1)} \beta_1^{(0)} + \beta_2^{(1)} \beta_2^{(0)}\right), \tag{C33}$$

with $\beta_1^{(0)} = \sqrt{4!} K_{\text{corr}}$ and $\beta_2^{(0)} = 6\sqrt{2} K_{\text{corr}}$.

2. Third-order effective Hamiltonian

The second order of the generator S is given by

$$S_2 = -\mathcal{L}\hat{V}_d(S_1), \tag{C34}$$

where V_d denotes the diagonal contributions of the perturbation Hamiltonian. In a first step we calculate $[V_d, S_1]$. Again with Eqs. (C20)–(C23) we get

$$\begin{aligned}[V_d, S_1] = \sqrt{2} \sum_{i,j=1}^{4} g_i^{\text{QB},c} \gamma_j^{(1)} \hat{Z}_i \hat{Z}_j \eta_{20}^{+} + \sum_{j=1}^{4} g_j^{\text{QB},c} \beta_1^{(1)} \left(\sqrt{5}\eta_{50}^{+} + 2\eta_{30}^{+}\right) + \sum_{j=1}^{4} g_j^{\text{QB},c} \beta_2^{(1)} \hat{Z}_j \left(\sqrt{3}\eta_{30}^{+} + \sqrt{2}\eta_{10}^{+}\right) + K_{\text{corr}} \\ \times \left(\sum_{j=1}^{4} \gamma_j^{(1)} A_1^{(4)} \hat{Z}_j \eta_{50}^{+} + \beta_1^{(1)} A_2^{(4)} \eta_{60}^{+} + \beta_2^{(1)} A_4^{(4)} \eta_{80}^{+} + \sum_{j=1}^{4} \gamma_j^{(1)} A_1^{(2)} \eta_{30}^{+} \beta_1^{(1)} A_2^{(2)} \eta_{40}^{+} + \beta_2^{(1)} A_4^{(2)} \eta_{60}^{+} \beta_2^{(1)} A_2^{(2)} \eta_{20}^{+} \right. \\ \left. + \sum_{j=1}^{4} \gamma_j^{(1)} A_1^{(0)} \hat{Z}_j \eta_{10}^{+} + \beta_1^{(1)} A_4^{(0)} \eta_{40}^{+} \beta_2^{(1)} A_2^{(0)} \eta_{20}^{+}\right).\end{aligned} \tag{C35}$$

The next order of the effective Hamiltonian is given by $H_{\text{eff},3} = b_1 P_0 \hat{S}_2(V_{\text{od}}) P_0$, so it is again sandwiched by projection operators onto the coupler ground state. S_2 is given by $-\mathcal{L}(V_d(S_1))$. $\mathcal{L}$ maps η_{ij}^{+} to η_{ij}^{-} and adds the respective energy prefactor $1/(E_i - E_j)$. Only terms proportional to η_{00} will not be projected to zero by P_0. From Eqs. (C20)–(C23) we see that only commutators of η's with identical indices will contribute. In V_{od} the only operators of this sort that appear are η_{10}, η_{20}, and η_{40}. This means that we can ignore all other η operators in the commutator $\hat{V}_d(S_1)$ since they do not contribute to $H_{\text{eff},3}$. Using this simplification, we get the following expression for the third-order effective Hamiltonian:

$$\hat{H}_{\text{eff},3} = \left[\sum_{i,j=1}^{4} \left(\frac{\sqrt{2}\beta_2^{(0)}}{(E_2 - E_0)} \gamma_i^{(1)} g_j^{\text{QB},c} + \frac{\sqrt{2}\beta_2^{(1)}}{E_1 - E_0} g_i^{\text{QB},c} g_i^{\text{QB},c} + \frac{K_{\text{corr}} A_1^{(0)}}{E_1 - E_0} \alpha_i^{(1)} g_j^{\text{QB},c}\right) \hat{Z}_i \hat{Z}_j + K_{\text{corr}} \hat{H}_{\text{shift}}^{(3)}\right], \tag{C36}$$

where $H_{\text{shift}}^{(3)}$ adds an overall energy shift to the coupler ground-state energy given by

$$H_{\text{shift}}^{(3)} = \sum_{j=1}^{4} \left(\frac{\beta_1^{(1)} \beta_1^{(0)} A_2^{(2)}}{E_4 - E_0} + \frac{\beta_2^{(1)} \beta_2^{(0)} A_2^{(2)}}{E_2 - E_0} + \frac{\beta_1^{(1)} \beta_1^{(0)} A_4^{(0)}}{E_4 - E_0} + \frac{\beta_2^{(1)} \beta_2^{(0)} A_2^{(0)}}{E_2 - E_0}\right). \tag{C37}$$

Hence, the third-order effective Hamiltonian has two effects on the qubits. It leads to an overall energy shift given by $H_{\text{shift}}^{(3)}$ and, like the second-order effective Hamiltonian, induces two-body local interactions. Therefore, we have to calculate the next higher order and see if local interactions $k > 2$ appear.

3. Fourth-order effective Hamiltonian

The third part of the generator is given by

$$S_3 = -\mathcal{L}\hat{V}_d(S_2) + a_2 \mathcal{L}\hat{S}_1^2(V_{\text{od}}), \tag{C38}$$

with

$$a_n = \frac{2^n B_n}{n!}. \tag{C39}$$

We start with calculating $\hat{V}_d S_2$. In the expression for $H_{\text{eff},4}$ the commutator of S_3 with V_{od} appears. This expression is again sandwiched by P_0 operators. In the same manner as in the last section we therefore have to include only terms of S_3 proportional to η_{10}, η_{40}, or η_{20}. This leads to 12 different terms. The effective Hamiltonian is given by

$$H_{\text{eff},4} = b_1 P_0 \hat{S}_3(V_{\text{od}}) P_0 + b_3 P_0 \hat{S}_1^3(V_{\text{od}}). \tag{C40}$$

We split this Hamiltonian into three different parts:

$$\begin{aligned} H_{\text{eff},4} &= H_{\text{eff},4}^{(1)} + H_{\text{eff},4}^{(2)} + H_{\text{eff},4}^{(3)} \\ &= -b_1 P_0 \left[\mathcal{L}\hat{V}_d(S_2), V_{\text{od}}\right] P_0 + b_1 a_2 P_0 \left[\mathcal{L}\hat{S}_1^2(V_{\text{od}}), V_{\text{od}}\right] + b_3 P_0 \hat{S}_1^3(V_{\text{od}}) P_0. \end{aligned} \tag{C41}$$

For the first part we get

$$\begin{aligned} H_{\text{eff},4}^{(1)} = -2b_1 K_{\text{corr}} \sum_{i,j=1}^{4} \Bigg[& \frac{5\beta_1^{(1)} g_i^{\text{QB},c} g_j^{\text{QB},c}}{(E_5 - E_0)(E_4 - E_0)} + \frac{\sqrt{5} K_{\text{corr}} A_1^{(4)} \gamma_i^{(1)} g_i^{\text{QB},c}}{(E_5 - E_0)(E_4 - E_0)} + \left(\frac{\sqrt{4}}{E_4 - E_0} + \frac{\sqrt{3}}{E_3 - E_0} \right) \frac{\sqrt{3}\beta_2^{(1)} g_i^{\text{Qb,c}} g_j^{\text{QB},c}}{E_3 - E_0} \\ & + \frac{K_{\text{corr}} A_1^{(2)} \gamma_i^{(1)} g_j^{\text{QB},c}}{E_3 - E_0} \left(\frac{\sqrt{4}}{E_4 - E_0} + \frac{\sqrt{3}}{(E_3 - E_0)} \right) + \frac{2\beta_1^{(1)} g_i^{\text{QB},c} g_j^{\text{QB},c}}{E_3 - E_0} \left(\frac{\sqrt{4}}{E_4 - E_0} + \frac{\sqrt{3}}{E_2 - E_0} \right) \\ & + \frac{2\beta_2^{(1)} \gamma_i^1 g_j^{\text{QB},c}}{(E_2 - E_0)^2} + \frac{\sqrt{2} K_{\text{corr}} A_1^{(0)} \gamma_i^{(1)} \gamma_j^{(1)}}{E_2 - E_0} + \frac{\sqrt{2} K_{\text{corr}} A_2^{(2)} \gamma_i^{(1)} g_j^{\text{QB},c}}{(E_2 - E_0)(E_4 - E_0)} + \frac{\sqrt{2} K_{\text{corr}} A_2^{(0)} \gamma_i^{(1)} g_j^{\text{QB},c}}{(E_2 - E_0)^2} \Bigg] \hat{Z}_i \hat{Z}_j \\ & + \sum_{j=1}^{4} \Bigg(\frac{\sqrt{2} K_{\text{corr}} \beta_2^{(1)} A_2^{(2)} g_j^{\text{QB},c}}{(E_2 - E_0)(E_1 - E_0)} + \frac{\sqrt{2} K_{\text{corr}} \beta_2^{(1)} A_2^{(0)} g_j^{\text{QB},c}}{(E_2 - E_0)(E_1 - E_0)} + \frac{\sqrt{5} K_{\text{corr}} \beta_1^{(1)} A_1^{(4)} g_j^{\text{QB},c}}{(E_5 - E_0)(E_1 - E_0)} + \frac{K_{\text{corr}} A_1^4 A_1^{(4)} \gamma_j^{(1)}}{(E_5 - E_0)(E_1 - E_0)} \\ & + \frac{2K_{\text{corr}} \beta_1^{(1)} A_1^{(2)} g_j^{\text{QB},c}}{(E_3 - E_0)(E_2 - E_0)} + \frac{\sqrt{3} K_{\text{corr}} \beta_2^{(1)} A_1^{(2)} g_j^{\text{QB},c}}{(E_3 - E_0)(E_1 - E_0)} + \frac{K_{\text{corr}} A_1^{(2)} A_1^{(2)} \gamma_j^{(1)}}{(E_3 - E_0)(E_1 - E_0)} + \frac{\sqrt{2} A_1^{(0)} \beta_2^{(1)} g_j^{\text{QB},c}}{(E_1 - E_0)^2} \\ & + \frac{K_{\text{corr}} A_1^{(0)} A_1^{(0)} \gamma_j^{(1)}}{(E_1 - E_0)^2} \Bigg) \hat{Z}_j + \frac{K_{\text{corr}}^2 A_2^{(4)} \beta_2^{(1)} A_2^{(4)}}{(E_6 - E_0)(E_2 - E_0)} + \frac{K_{\text{corr}}^2 \beta_2^{(1)} A_4^{(2)} A_2^{(2)}}{(E_2 - E_0)(E_4 - E_0)} + \frac{K_{\text{corr}}^2 \beta_2^{(1)} A_2^{(0)} A_2^{(2)}}{(E_2 - E_0)(E_4 - E_0)} \\ & + \frac{K_{\text{corr}}^2 \beta_1^{(1)} A_2^{(2)} A_2^{(2)}}{(E_4 - E_0)(E_2 - E_0)} + \frac{K_{\text{corr}}^2 \beta_1^{(1)} A_4^{(0)} A_2^{(2)}}{(E_4 - E_0)(E_2 - E_0)} + \frac{K_{\text{corr}}^2 \beta_1^{(1)} A_2^{(4)} A_4^{(2)}}{(E_6 - E_0)(E_4 - E_0)} + \frac{K_{\text{corr}}^2 \beta_2^{(1)} A_4^{(2)} A_4^{(2)}}{(E_6 - E_0)(E_4 - E_0)} \\ & + \frac{K_{\text{corr}}^2 A_2(0) \beta_2^{(1)} A_2^{(2)}}{(E_2 - E_0)^2} + \frac{K_{\text{corr}} \beta_2^{(1)} A_2^{(0)} A_2^{(0)}}{(E_2 - E_0)^2} + \frac{K_{\text{corr}} \beta_1^{(1)} A_4^{(0)} A_2^{(2)}}{(E_4 - E_0)^2} + \frac{K_{\text{corr}} \beta_1^{(1)} A_4^{(0)} A_4^{(0)}}{(E_4 - E_0)^2} \\ & + \frac{K_{\text{corr}}^2 \beta_1^{(1)} A_2^{(4)} A_2^{(4)}}{(E_6 - E_0)(E_2 - E_0)} + \frac{K_{\text{corr}}^2 \beta_2^{(1)} A_4^{(4)} A_4^{(4)}}{(E_8 - E_0)(E_4 - E_0)} + \sum_{i,j,k=1}^{4} \frac{2K_{\text{corr}} \gamma_i^{(1)} g_j^{\text{QB},c} g_k^{\text{QB},c}}{(E_2 - E_0)(E_1 - E_0)} \hat{Z}_i \hat{Z}_j \hat{Z}_k. \end{aligned} \tag{C42}$$

We see that a lot of two-body local coupling terms arise. Additionally we have single $\hat{Z}$ corrections, an overall energy shift, and most importantly the last term leads to three local qubi-qubit interactions. We first calculate the other contributions to the effective Hamiltonian. The second part is given by

$$\begin{aligned} H_{\text{eff},4}^{(2)} = 2b_1 a_1 \Bigg[& 4 \sum_{i,j,k,l=1}^{3} \frac{g_i^{\text{QB},c} g_j^{\text{QB},c} g_k^{\text{QB},c} g_l^{\text{QB},c}}{(E_1 - E_0)^4} \hat{Z}_i \hat{Z}_j \hat{Z}_k \hat{Z}_l + \sum_{i,j=1}^{4} \Bigg(\frac{\gamma_i^{(1)} \gamma_j^{(1)} \beta_1^{(0)} \beta_1^{(0)}}{E_4 - E_0} + \frac{\gamma_i^{(1)} \gamma_j^{(1)} \beta_2^{(0)} \beta_2^{(0)}}{E_2 - E_0} \\ & + \frac{\beta_1^{(0)} \beta_1^{(1)} \gamma_i^{(1)} g_j^{\text{QB},c}}{E_4 - E_0} + 2\beta_1^{(1)} \beta_1^{(0)} \gamma_i^{(1)} \gamma_j^{(1)} + \frac{\beta_2^{(0)} \beta_2^{(0)} \gamma_i^{(1)} g_j^{\text{QB},c}}{E_2 - E_0} + 2\beta_2^{(1)} \beta_2^{(0)} \gamma_i^{(1)} \gamma_j^{(1)} \end{aligned}$$

$$+\frac{2\beta_2^{(1)}\beta_2^{(0)}\gamma_i^{(1)}g_j^{\mathrm{QB},c}}{E_2-E_0}+\beta_2^{(1)}\beta_2^{(0)}\beta_2^{(0)}\gamma_i^{(1)}\gamma_j^{(1)}+\beta_2^{(1)}\beta_2^{(1)}\gamma_i^{(1)}g_j^{\mathrm{QB},c}+\frac{2\beta_1^{(1)}\beta_1^{0}\gamma_i^{(1)}g_j^{\mathrm{QB},c}}{E_4-E_0}$$
$$+\beta_1^{(1)}\beta_1^{(1)}\gamma_i^{(1)}g_j^{\mathrm{QB},c}+\beta_1^{(1)}\beta_1^{(0)}\gamma_i^{(1)}\gamma_j^{(1)}\Big)\hat{Z}_i\hat{Z}_j+\frac{\beta_2^{(1)}\beta_1^{(1)}\beta_2^{(0)}\beta_1^{(0)}}{E_4-E_0}+\frac{2\beta_1^{(1)}\beta_1^{(0)}\beta_2^{(1)}\beta_2^{(0)}}{E_2-E_0}$$
$$+\frac{4\beta_1^{(1)}\beta_1^{(1)}\beta_1^{(0)}\beta_1^{(0)}}{E_4-E_0}+\frac{\beta_2^{(1)}\beta_2^{(1)}\beta_1^{(0)}\beta_1^{(0)}}{E_4-E_0}+\frac{\beta_1^{(1)}\beta_1^{(1)}\beta_2^{(0)}\beta_2^{(0)}}{E_2-E_0}+\frac{\beta_2^{(1)}\beta_1^{(0)}\beta_1^{1()}\beta_2^{(0)}}{E_2-E_0}+\frac{2\beta_1^{(1)}\beta_2^{(1)}\beta_2^{(0)}\beta_1^{(0)}}{E_4-E_0}\Bigg] \tag{C43}$$

and the last part reads

$$H_{\mathrm{eff},4}^{(3)}=2b_3\Bigg[4\sum_{i,j,k,l=1}^{4}\gamma_i^{(1)}\gamma_j^{(1)}\gamma_k^{(1)}g_l^{\mathrm{QB},c}\hat{Z}_i\hat{Z}_j\hat{Z}_k\hat{Z}_l+\sum_{i,j=}^{4}(\beta_1^{(0)}\beta_1^{(1)}\gamma_i^{(1)}\gamma_j^{(1)}+\beta_2^{(0)}\beta_2^{(1)}\gamma_i^{(1)}\gamma_j^{(1)}+\beta_1^{(1)}\beta_1^{(1)}\gamma_i^{(1)}g_j^{\mathrm{QB},c}$$
$$+2\beta_1^{(0)}\beta_1^{(0)}\gamma_i^{(1)}\gamma_j^{(1)}+\beta_2^{(1)}\beta_2^{(1)}\gamma_i^{(1)}g_j^{\mathrm{QB},c}+2\beta_2^{(0)}\beta_2^{(1)}\gamma_i^{(1)}\gamma_j^{(1)}+2\beta_2^{(1)}\beta_2^{(1)}\gamma_i^{(1)}g_j^{\mathrm{QB},c}+\beta_2^{(0)}\beta_2^{(1)}\gamma_i^{(1)}\gamma_j^{(1)}$$
$$+\beta_2^{(1)}\beta_2^{(1)}\gamma_i^{(1)}g_j^{\mathrm{Qb,c}})\hat{Z}_i\hat{Z}_j+2\beta_1^{(1)}\beta_1^{(0)}\beta_2^{(1)}\beta_2^{(1)}+\beta_2^{(1)}\beta_1^{(1)}\beta_2^{(0)}\beta_1^{(1)}+\beta_2^{(1)}\beta_2^{(1)}\beta_1^{(0)}\beta_1^{(1)}4\beta_2^{(1)}\beta_2^{(1)}\beta_2^{(0)}\beta_2^{(1)}$$
$$+4\beta_1^{(1)}\beta_1^{(1)}\beta_1^{(0)}\beta_1^{(1)}+\beta_1^{(1)}\beta_1^{(1)}\beta_2^{(0)}\beta_2^{(1)}+\beta_1^{(1)}\beta_2^{(1)}\beta_1^{(0)}\beta_2^{(1)}+2\beta_1^{(1)}\beta_2^{(0)}\beta_2^{(0)}\beta_1^{(0)}\Bigg]. \tag{C44}$$

Finally, with all these results, the fourth-order effective Hamiltonian acting only on the coupler ground-state subspace can be written as

$$H_{\mathrm{eff}}=\hat{P}_0\hat{H}_0\hat{P}_0+\hat{P}_0\hat{V}\hat{P}_0+\sum_{n=2}^{4}\hat{H}_{\mathrm{eff},n}. \tag{C45}$$

4. Coupling strengths

$H_{\mathrm{eff},4}$ leads to three and four local qubit-qubit interactions. There are still two local qubit interactions present and we want the higher ones to give the leading effect. Therefore, it is necessary to go to a regime where the two local interactions vanish or at least are smaller than the higher ones. The sum $\sum_{i,j,k,l}$ also gives rise to two local interactions (e.g., if $i=j$ and $k=l$), so we also have to take them into account.

To summarize the results, we want to give expressions for the different couplings. For simplification we assume that the qubit parameters are the same for all qubits. We define the different coupling strengths such that we can write the effective interaction Hamiltonian as

$$H_{\mathrm{int,\,eff}}=J_4\hat{\hat{Z}}_1\hat{Z}_2\hat{Z}_3\hat{Z}_4+J_3\sum_{i<j<k}\hat{Z}_i\hat{Z}_j\hat{Z}_k+J_2\sum_{i<k}\hat{Z}_i\hat{Z}_j+J_1\sum_{i=1}^{4}\hat{Z}_i,$$

where the whole interaction Hamiltonian acts only on the $|0\rangle$ subspace of the coupler. The restriction of the sums comes from the fact that, for example, $\hat{Z}_i\hat{Z}_j=\hat{Z}_j\hat{Z}_i$, and hence we get an additional prefactor in the different coupling terms:

$$\sum_{i\neq j\neq k\neq l}\hat{\mathrm{Z}}_i\hat{Z}_j\hat{Z}_k\hat{Z}_l+\sum_{i\neq j\neq k}\hat{Z}_i\hat{Z}_j\hat{Z}_k+\sum_{i\neq k}\hat{Z}_i\hat{Z}_j+\sum_{i=1}^{4}\hat{Z}_i$$
$$=4!\hat{Z}_i\hat{Z}_j\hat{Z}_k\hat{Z}_l+3!\sum_{i<j<k}\hat{Z}_i\hat{Z}_j\hat{Z}_k+2!\sum_{i<k}\hat{Z}_i\hat{Z}_j+\sum_{i=1}^{4}\hat{Z}_i. \tag{C46}$$

The four-body coupling strength is given by

$$J_4=24\frac{g_{\mathrm{QB},c}^4}{\Delta_{10}^3}, \tag{C47}$$

with $\Delta_{ij} = E_i - E_j$. The three-body coupling strength is given by

$$J_3 = -6\frac{2K_{\mathrm{corr}}g_{\mathrm{QB},c}^3}{\Delta_{20}\Delta_{10}^2}. \tag{C48}$$

The expression for the two-body interaction is a little-more complicated,

$$\begin{aligned}
J_2/2 = g_{\mathrm{QB,QB}}/2 &- \frac{g_{\mathrm{QB},c}^2}{\Delta_{10}} + \frac{12K_{\mathrm{corr}}g_{\mathrm{QB},c}^2}{\Delta_{20}\Delta_{10}} + \frac{12K_{\mathrm{corr}}g_{\mathrm{QB},c}^2}{\Delta_{10}\Delta_{20}} + \frac{12K_{\mathrm{corr}}g_{\mathrm{QB},c}^2}{\Delta_{10}^2} - \frac{10\sqrt{6}K_{\mathrm{corr}}^2g_{\mathrm{QB},c}^2}{\Delta_{50}\Delta_{40}^2} - \frac{10\sqrt{6}K_{\mathrm{corr}}^2g_{\mathrm{QB},c}^2}{\Delta_{50}\Delta_{40}\Delta_{10}} \\
&- \frac{12\sqrt{6}K_{\mathrm{corr}}^2g_{\mathrm{QB},c}^2}{\Delta_{40}\Delta_{30}\Delta_{20}} - \frac{18\sqrt{2}K_{\mathrm{corr}}^2g_{\mathrm{QB},c}^2}{\Delta_{30}^2\Delta_{20}} - \frac{20\sqrt{6}K_{\mathrm{corr}}^2g_{\mathrm{QB},c}^2}{\Delta_{40}\Delta_{30}\Delta_{10}} - \frac{30\sqrt{2}K_{\mathrm{corr}}^2g_{\mathrm{QB},c}^2}{\Delta_{30}^2\Delta_{10}} - \frac{8\sqrt{6}K_{\mathrm{corr}}^2g_{\mathrm{QB},c}^2}{\Delta_{40}\Delta_{20}\Delta_{10}} - \frac{12\sqrt{2}K_{\mathrm{corr}}^2g_{\mathrm{QB},c}^2}{\Delta_{20}^3} \\
&- \frac{12\sqrt{2}K_{\mathrm{corr}}^2g_{\mathrm{QB},c}}{\Delta_{20}\Delta_{10}^2} - \frac{28\sqrt{8}K_{\mathrm{corr}}^2g_{\mathrm{QB},c}}{\Delta_{40}\Delta_{20}\Delta_{10}} - \frac{36\sqrt{2}K_{\mathrm{corr}}^2g_{\mathrm{QB},c}^2}{\Delta_{20}^2\Delta_{10}} + \frac{8K_{\mathrm{corr}}^2g_{\mathrm{QB},c}^2}{\Delta_{40}\Delta_{10}^2} + \frac{24K_{\mathrm{corr}}^2g_{\mathrm{QB},c}^2}{\Delta_{20}^3} + \frac{8K_{\mathrm{corr}}^2g_{\mathrm{QB},c}^2}{\Delta_{40}^2\Delta_{10}} \\
&+ \frac{16K_{\mathrm{corr}}^2g_{\mathrm{QB},c}^2}{\Delta_{10}^3} + \frac{48K_{\mathrm{corr}}^2g_{\mathrm{QB},c}}{\Delta_{20}^3} + \frac{48K_{\mathrm{corr}}^2g_{\mathrm{QB},c}^2}{\Delta_{20}\Delta_{10}^2} + \frac{48K_{\mathrm{corr}}^2g_{\mathrm{QB},c}^2}{\Delta_{20}^2\Delta_{10}} + \frac{144\sqrt{2}K_{\mathrm{corr}}^2g_{\mathrm{QB},c}}{\Delta_{10}^2\Delta_{20}} + \frac{24K_{\mathrm{corr}}^2g_{\mathrm{QB},c}^2}{\Delta_{10}\Delta_{20}^2} \\
&+ \frac{48K_{\mathrm{corr}}^2g_{\mathrm{QB},c}^2}{\Delta_{40}\Delta_{10}\Delta_{20}} + \frac{24K_{\mathrm{corr}}^2g_{\mathrm{QB},c}}{\Delta_{10}\Delta_{20}^2} + \frac{24K_{\mathrm{corr}}^2g_{\mathrm{QB},c}^2}{\Delta_{10}^2\Delta_{20}} - \frac{2K_{\mathrm{corr}}^2g_{\mathrm{QB},c}^2}{\Delta_{40}\Delta_{10}^2} - \frac{6K_{\mathrm{corr}}^2g_{\mathrm{QB},c}^2}{\Delta_{10}^2\Delta_{20}} - \frac{2K_{\mathrm{corr}}^2g_{\mathrm{QB},c}^2}{\Delta_{10}\Delta_{40}^2} \\
&- \frac{4K_{\mathrm{corr}}^2g_{\mathrm{QB},c}^2}{\Delta_{10}^2\Delta_{40}} - \frac{6K_{\mathrm{corr}}^2g_{\mathrm{QB},c}^2}{\Delta_{10}\Delta_{20}^2} - \frac{12K_{\mathrm{corr}}^2g_{\mathrm{QB},c}^2}{\Delta_{10}^2\Delta_{20}} - \frac{12K_{\mathrm{corr}}^2g_{\mathrm{QB},c}^2}{\Delta_{10}^2\Delta_{20}} - \frac{6K_{\mathrm{corr}}^2g_{\mathrm{QB},c}^2}{\Delta_{10}^2\Delta_{20}} - \frac{6K_{\mathrm{corr}}^2g_{\mathrm{QB},c}^2}{\Delta_{10}\Delta_{20}^2} \\
&- \frac{2K_{\mathrm{corr}}^2g_{\mathrm{QB},c}^2}{\Delta_{10}\Delta_{20}^2} + \frac{20g_{\mathrm{QB},c}^4}{\Delta_{10}^3},
\end{aligned} \tag{C49}$$

as are the $\hat{Z}$ corrections,

$$\begin{aligned}
J_1 = &- \frac{72\sqrt{3}K_{\mathrm{corr}}^3g_{\mathrm{QB},c}}{\Delta_{20}^2\Delta_{10}} - \frac{432K_{\mathrm{corr}}^3g_{\mathrm{QB},c}}{\Delta_{20}^2\Delta_{10}} \\
&- \frac{120\sqrt{3}K_{\mathrm{corr}}^3g_{\mathrm{QB},c}}{\Delta_{50}\Delta_{40}\Delta_{10}} - \frac{120K_{\mathrm{corr}}^3g_{\mathrm{QB},c}}{\Delta_{50}\Delta_{10}^2} \\
&- \frac{240K_{\mathrm{corr}}^3g_{\mathrm{QB},c}}{\Delta_{30}\Delta_{40}\Delta_{10}} - \frac{360K_{\mathrm{corr}}^3g_{\mathrm{QB},c}}{\Delta_{30}\Delta_{20}\Delta_{10}} \\
&- \frac{600K_{\mathrm{corr}}^3g_{\mathrm{QB},c}}{\Delta_{30}\Delta_{10}^2} - \frac{144K_{\mathrm{corr}}^3g_{\mathrm{QB},c}}{\Delta_{20}\Delta_{10}^2} \\
&- \frac{144K_{\mathrm{corr}}^3g_{\mathrm{QB},c}}{\Delta_{10}^3} - 12\frac{K_{\mathrm{corr}}g_{\mathrm{QB},c}^3}{\Delta_{10}^3}.
\end{aligned} \tag{C50}$$

The bare-coupler Hamiltonian is equivalent to a harmonic oscillator, such that $\Delta_{n0} = (n-1)\Delta_{10}$ is satisfied. Therefore, we can simplify the expressions for the coupling strengths:

$$J_4 = 24\frac{g_{\mathrm{QB},c}^4}{\Delta_{10}^3}, \tag{C51}$$

$$J_3 = -6\frac{K_{\mathrm{corr}}g_{\mathrm{QB},c}^3}{\Delta_{10}^3}, \tag{C52}$$

$$\begin{aligned}
J_2 = g_{\mathrm{QB,QB}} - 2\Bigg(1 &- \frac{1}{4}\frac{K_{\mathrm{corr}}}{\Delta_{10}} \\
&- \underbrace{\frac{1689 + 1060\sqrt{2} - 82\sqrt{6} - 12\sqrt{30}}{24}}_{\approx 122}\frac{K_{\mathrm{corr}}^2}{\Delta_{10}^2}\Bigg)\frac{g_{\mathrm{QB},c}^2}{\Delta_{10}} \\
&+ 40\frac{g_{\mathrm{QB},c}^4}{\Delta_{10}^3},
\end{aligned} \tag{C53}$$

$$J_1 = -\underbrace{\left(628 + 24\sqrt{3}\right)}_{\approx 670}\frac{K_{\mathrm{corr}}^3g_{\mathrm{QB},c}}{\Delta_{10}^3} - 12\frac{K_{\mathrm{corr}}g_{\mathrm{QB},c}^3}{\Delta_{10}^3}. \tag{C54}$$

Putting in the expressions for K_{corr}, $g_{\mathrm{QB},c}$ and Δ_{10}, we can write the different couplings in terms of system

parameters:

$$J_4 = 3E_{\tilde{L}_c}\frac{(\alpha s)^4}{\zeta_c(1-\beta_c)^{5/2}}, \tag{C55}$$

$$J_3 = -E_{\tilde{L}_c}\frac{(\alpha s)^3\beta_c\sqrt{\zeta_c}}{32(1-\beta_c)^3}, \tag{C56}$$

$$J_2 = E_{\tilde{L}_c}(\alpha s)^2\left(1-\frac{1}{(1-\beta_c)}+\frac{1}{2}\frac{\beta_c\zeta_c}{(1-\beta_c)^{5/2}} + c_1\frac{\beta_c^2\zeta_c^2}{(1-\beta_c)^4}+5\frac{(\alpha s)^2}{\zeta_c(1-\beta_c)^{5/2}}\right), \tag{C57}$$

with $c_1 = (1689+1060\sqrt{2}-82\sqrt{6}-12\sqrt{30})/55\,296$ and where we assume we have identical qubits, such that $\alpha_i = \alpha_j = \alpha$, $s_i = s_j = s$. All these expressions diverge for $\beta_c \longrightarrow 1$. This is since the prefactors of H_{int} (especially $V_{\text{QB},c}$) are on the order of 1 in this case, such that the convergence criteria for the Schrieffer-Wolff expansion is no longer satisfied. In Appendix D, we get very interesting effect in the regime $\beta_c < 0.6$. J_1 and J_3 are 2–3 orders of magnitude smaller than the equal contributions; hence, they can be ignored (also observed in the numerical simulations).

APPENDIX D: NUMERICAL EVALUATION OF THE SWT

In Appendix C, we present an analytical solution for the SWT by truncation of the cosine part of the coupler potential. To get more-accurate results, it is more convenient to include the full coupler potential and solve for the eigenfunctions numerically. We see that corrections from higher-order cosine terms play an important role for larger nonlinearities. To do so, we numerically solve the bare-coupler Hamiltonian:

$$\hat{H}_c = 4E_{\tilde{L}_c}\xi_c^2\frac{q_c^2}{2}+\frac{\hat{\varphi}}{2}+\beta_c\cos\hat{\varphi}_c. \tag{D1}$$

This Hamiltonian can be evolved in harmonic oscillator states. For the harmonic part we use the results from Appendix C. The cosine part can be written down in this basis using the relation

$$\langle n|e^{ir(\hat{a}^\dagger+\hat{a})}|m\rangle = i^{3n+m}\sqrt{\frac{n!}{m!}}e^{-\frac{r^2}{2}}r^{n-k}L_n^{(n-m)}r^2, \tag{D2}$$

where $L_j^{(n-m)}$ refers to the generalized Laguerre polynomial. The cosine part of the potential can now be written in the polar representation, and we can write down $\hat{H}_c$ in the harmonic oscillator basis:

$$\hat{H}_c = \sum_{n,m=1}^{\infty}\langle n|\hat{H}_c|m\rangle\,|n\rangle\,\langle m|\,. \tag{D3}$$

Solving for the eigenvectors, we find the unitary transformation $\hat{U}_c$ that diagonalizes $\hat{H}_c$. With U it is possible,to transform the interaction part of the Hamiltonian into the eigensystem of $\hat{H}_c$ [the coupler parts of the interaction can easily be written down in the harmonic oscillator basis using Eq. (D2)]. This makes it easy to numerically calculate the commutators arising during the SWT by simple matrix multiplications. We truncate the series (D3) at $n = 40$ oscillator states, since higher truncation limits do not lead to any notable changes of the results. With this we can calculate the prefactors of Eq. (C46). We see that the results of the analytical SWT and the numerical SWT show the same overall behavior, but the values of both are significantly different. Since the cosine part of the potential gives important contributions to the value of the energy gap, this is what we expect. For increasing β_c, $t\omega_c$, which denotes the gap in the analytical cas,e decreases rapidly, pushing the calculation over the convergence limit of the SWT. By including the whole potential in the numerical case, we find the decrease of the gap with increasing β_c is much slower, leading a large shift of the convergence breakdown to higher values of β_c.

APPENDIX E: DISCUSSION OF THE SWT

As mentioned in the main text, there are rather large deviations between the coupling strengths of the effective Hamiltonian obtained by the SWT and the completely numerically determined coupling strengths. The SWT gives the right-principle behavior of the coupling, meaning a change of J_2 from antiferromagnetic to ferromagnetic due to the indirect-coupling part of the Hamiltonian and a continuous increase of J_4. There are two main problems why the SWT does not quantitatively model the effective system Hamiltonian. The first one is as mentioned above, the way we model the qubit. As shown in Sec. B, we model the qubit potential with two shifted harmonic potentials. The smaller the qubit nonlinearity β_j, the further away the actual potential is from the double well. To get qualitative results, we would have to include higher-order corrections to the potential, but then it is no longer possible to get nice analytical results. On the other hand, the more we increase the nonlinearity of the coupler β_c, the more higher orders of the SWT matter. This is because the energy distance between the coupler ground-state subspace and coupler excited-state subspace decreases with increasing coupler nonlinearity; hence, prefactors of, for example, sixth-order terms increase. This is the reason for the turnover of the coupling strengths at $\beta_c \approx 0.5$ (see Fig. 3), which we do not see in the full numerical results

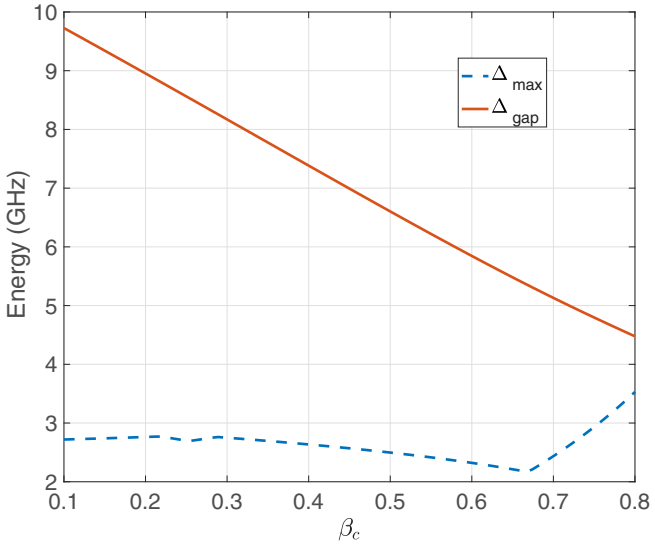

FIG. 7. Gap between coupler ground-state subspace and coupler excited-state subspace Δ_{gap} and dependence of the maximum spectral distance in coupler ground-state subspace Δ_{max} on the coupler nonlinearity β_c.

(see Fig. 2). Also, for too-strong nonlinearities when the two subspaces start to mix, the SWT will diverge when we do not include the coupler excited-state subspace as well. But as soon as these subspaces start to mix, the system can no longer mimic the spectrum of the general Ising Hamiltonian including four local interactions; hence, we are not interested in this regime. Here by "mix" we mean that the gap between the two coupler subspaces becomes comparable to the gaps of the spectral lines in the coupler ground-state subspace. Then it is likely that interactions between the two subspaces happen. In Fig. 7 we show the gap between the lowest state in the coupler excited-state subspace and the highest state in the coupler ground-state subspace and the dependence of the maximum distance between two spectral lines in the coupler ground-state subspace on the coupler nonlinearity β_c. For consistency, we chose the same qubit and coupler parameters as in Fig. 2. We sees that for small β_c, the gap is much larger than the intersubspace energy differences, but for increasing β_c, the gap starts to decrease, whereas the intersubspace energy difference increases. In the region $0.7 < \beta_c < 0.8$ the two values of Δ_{max} and Δ_{gap} become comparable and the two subspaces are no longer well separated. This is the reason why we show coupling strengths β_c only up to 0.7 in Fig. 1.

APPENDIX F: FABRICATION ERRORS

Here we test the robustness of the our coupler against fabrication errors. For this purpose, we calculate several susceptibilities that describe the harm caused by fabrication errors (e.g., wrong junction parameters).

For every system parameter that arises in the four-local-interaction and two-local-interaction strength, we can define a corresponding susceptibility:

$$\chi_{4J,j} = \frac{1}{J_4} \sum_{\text{junctions}} \left| \frac{\partial J_4}{\partial P_j} \right|_{J_4=\max}, \tag{F1}$$

$$\chi_{2J,j} = \frac{1}{J_2} \sum_{\text{junctions}} \left| \frac{\partial J_2}{\partial P_j} \right|_{J_2=\max}, \tag{F2}$$

where 2 and 4 denote the two-local-interaction strength and the four-local-interaction strength, respectively, and P_j represents the system parameter, which varies due to fabrication issues. All our analytical results seem to only qualitatively coincide with the numerical solution. Therefore, we calculate the susceptibilites in this article numerically. The two-local-interaction and four-local-interaction strengths can be extracted from the spectrum and then can be used to calculate the derivatives appearing in the susceptibilities. Here we assume that the optimal point is the one where the four-local-interaction strength is twice the two-local-interaction strength, so we vary the respective parameters around this optimal point.

1. Error in Josephson energy

A typical fabrication error is an impurity in the junctions included in the system. This leads to variations of the Josephson energy. First we study a variation of the Josephson energy of the qubit junctions:

$$\begin{aligned} \chi_{4,E_{J_j}} &= \frac{4}{J_4} \left| \frac{\partial J_4}{\partial E_{J_j}} \right| \\ &= \frac{4}{J_4} \left| \frac{\partial J_4}{\partial \beta_j} \right| \left| \frac{\partial \beta_j}{\partial E_{J_j}} \right| \\ &= \frac{4}{J_4} \left| \frac{\partial J_4}{\partial \beta_j} \right| \frac{1}{E_{\tilde{L}_c}}, \end{aligned} \tag{F3}$$

where we use the fact that only β_j changes if we change E_{J_j} and we assume equal parameters for all four qubits (factor 4). The derivative appearing in the expression can be calculated numerically, and $E_{\tilde{L}_c}$ will be a normalization parameter. In Fig. 8 we show the variation of the four local interactions and two local interactions for a small variation of E_{J_j}. The susceptibility for the two local interactions $\chi_{J_2,E_{J_j}}$ can be calculated analogously to $\chi_{J_4,E_{J_j}}$, but we additionally have to include a factor of 3, which arises from the fact that every qubit can interact with three other qubits. Here we show the variation of the coupling strength with the nonlinearity β_j, and using Fig. 8, we can extract

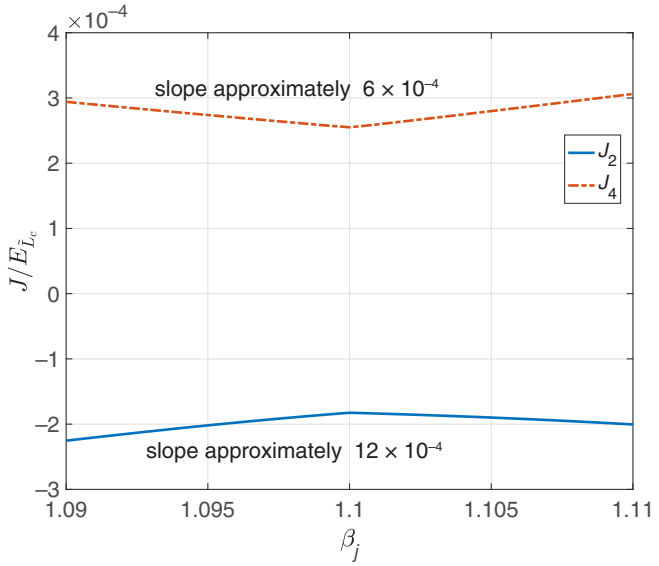

FIG. 8. Variation of the two and four local interactions with varying nonlinearity of the qubits. The slope can be extracted from the plots. We choose the same parameters as in the main text: $\chi_c = 0.01$, $\chi_j = 0.05$, and $\beta_c = 0.43$.

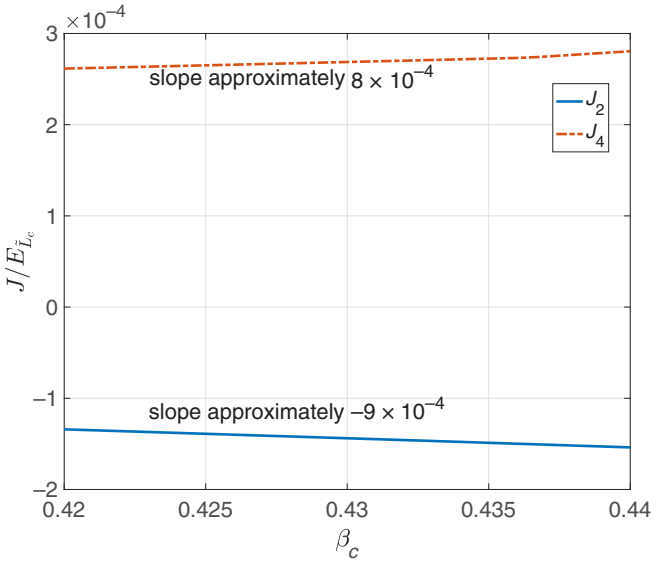

FIG. 9. Variation of the two and four local interactions with varying nonlinearity of the coupler. The slope can be extracted from the plots. We choose the same parameters as in the main text: $\chi_c = 0.01$, $\chi_j = 0.05$, and $\beta_c = 0.51$.

the derivatives $\partial J/\partial E_{J_j}$ we need to calculate the susceptibilites. This gives the following values for the system parameters used:

$$E_{\tilde{L}_c}\chi_{4J,E_{J_j}} \approx \frac{4}{J_4}6\times 10^{-4} \approx 2.1, \tag{F4}$$

$$E_{\tilde{L}_c}\chi_{2J,E_{J_j}} \approx \frac{12}{J_2}12\times 10^{-4} \approx 33.1. \tag{F5}$$

We see that the two local interactions are more affected by variations of the Josephson energies. However, $E_{\tilde{L}_c}$ is in the terahertz range for typical system parameters. This means that even for the two local interactions, changing E_{J_j} by about 1 GHz results in a change in the coupling strength on the order of only 0.1–1 GHz . Typical fabrication errors are assumed to be much smaller than 1 GHz, such that small variations do not crucially affect the two coupling strengths and the susceptibilities are rather small.

The same study can be done for a variation of the coupler's Josephson energy. The results are shown in Fig. 9, and again we can extract the derivative needed from Fig. 9 to get an approximate value for the susceptibilities:

$$E_{\tilde{L}_c}\chi_{4J,E_{J_c}} \approx \frac{1}{J_4}5\times 8^{-4} \approx 2.7, \tag{F6}$$

$$E_{\tilde{L}_c}\chi_{2J,E_{J_c}} \approx \frac{1}{J_2}4\times 9^{-4} \approx 6.2. \tag{F7}$$

As in the previous case, for typical values of $E_{\tilde{L}_c}$ these values of the susceptibilities lead to extremely small changes of the coupling strengths when E_{J_c} does not vary too much.

2. Error in inductive energy

Another typical fabrication error is a deviation of inductances between theoretical predicted and actual values in the experiment. In this case it is a little-more difficult to calculate the corresponding susceptibilities, since more than one parameter appearing in the coupling strength depends on the impedances of the qubits L_j and the coupler L_c, respectively. First we assume fabrication error in the coupler impedance, which means we have a change in $E_{\tilde{L}_c}$. The susceptibility can be written as

$$\begin{aligned}\chi_{4J,E_{L_c}} &= \frac{1}{J_4}\left(\left|\frac{\partial J_4}{\partial E_{\tilde{L}_c}}\right|\left|\frac{\partial E_{\tilde{L}_c}}{\partial \tilde{L}_c}\right|\left|\frac{\partial}{\tilde{L}_c}\partial L_c\right|\right.\\ &\quad\left.+\left|\frac{\partial J_4}{\partial x i_c}\right|\left|\frac{\xi_c}{\partial \tilde{L}_c}\right|\left|\frac{\partial}{\tilde{L}_c}\partial L_c\right|+\left|\frac{\partial J_4}{\partial \beta_c}\right|\left|\frac{\partial \beta_c}{\partial \tilde{L}_c}\right|\left|\frac{\partial}{\tilde{L}_c}\partial L_c\right|\right)\\ &= \frac{1}{\tilde{L}_c}\left(1+\chi_c\frac{1}{J_4}\left|\frac{\partial J_4}{\partial \xi_c}\right|+\beta_c\left|\frac{\partial J_4}{\partial \beta_c}\right|\right)\\ &\Rightarrow \tilde{L}_c\chi_{4J,L_c} = 1+\chi_c\frac{1}{J_4}\left|\frac{\partial J_4}{\partial \xi_c}\right|+\beta_c\left|\frac{\partial J_4}{\partial \beta_c}\right|.\end{aligned} \tag{F8}$$

Again we can plot the variation of the coupling strength around the optimal point to numerically determine the two derivatives appearing in the expression for χ. The susceptibility for the two local interactions is analogous, and we just have to replace J_4 with J_2. The variation with β_c is shown in Fig. 9, and in Fig. 10 we see the variation of the coupling strengths with ξ_c. For the two susceptibilities we

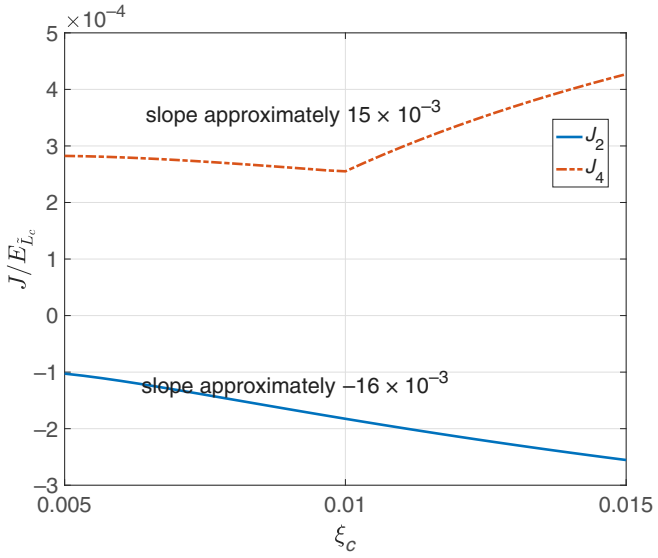

FIG. 10. Variation of the two and four local interactions with varying ξ_c. The slope can be extracted from the plots. We choose the same parameters as in the main text: $\chi_c = 0.01$, $\chi_j = 0.05$, and $\beta_c = 0.51$.

get the approximate values

$$\tilde{L}_c \chi_{4J,L_c} \approx 1.5, \tag{F9}$$

$$\tilde{L}_c \chi_{2J,L_c} \approx 2.1. \tag{F10}$$

However, these susceptibilities are given with respect to $\tilde{L}_c$. It is more convenient to look at the susceptibilities with respect to the inductive energies $E_{\tilde{L}_c}$ and E_{L_j}, respectively. We start with the first one to see how a change in $E_{\tilde{L}_c}$ affects the coupling strength. The corresponding susceptibility is given by (we choose units such that $J_i = E_{\tilde{L}_c} \tilde{J}_i$)

$$E_{\tilde{L}_c} \chi_{4J,E_{\tilde{L}_c}} = 1, \tag{F11}$$

$$E_{\tilde{L}_c} \chi_{2J,E_{\tilde{L}_c}} = 4, \tag{F12}$$

where again the factor of 4 in J_2 arises from the fact that four qubits interact with the coupler. A change in the inductive energy of the qubits leads to a change of β_j, such that

$$\begin{aligned} \chi_{4J,E_{L_j}} &= \frac{4}{J_4} \left(\left| \frac{\partial J_4}{\partial \beta_j} \right| \left| \frac{\partial \beta_j}{\partial E_{L_j}} \right| \right) \\ &= \frac{4}{J_4} \frac{\beta_j}{E_{L_j}} \left| \frac{\partial J_4}{\beta_j} \right|; \end{aligned} \tag{F13}$$

hence, we get (using Fig. 8)

$$E_{L_j} \chi_{4J,E_{L_j}} \approx 9, \tag{F14}$$

$$E_{L_j} \chi_{2J,E_{L_j}} \approx 36. \tag{F15}$$

We see that these two susceptibilities are the most-critical ones, since E_{L_j} is 1–2 orders of magnitude smaller than $E_{\tilde{L}_c}$. The fabrication error of inductances is usually much smaller than the corresponding errors in the junction and we still need a huge discrepancy here to get a significant change of the coupling strengths (since E_{L_j} is still on the order of 10–100 GHz).

To summarize the susceptibility results, we show that only huge fabrication errors of the junctions as well as the inductances lead to significant changes of the coupling strengths. Hence, our coupler setup is assumed to be robust against fabrication errors.

[1] Edward Farhi, Jeffrey Goldstone, Sam Gutmann, and Michael Sipser, Quantum computation by adiabatic evolution, arXiv:quant-ph/0001106 (2000).

[2] Edward Farhi, Jeffrey Goldstone, Sam Gutmann, Joshua Lapan, Andrew Lundgren, and Daniel Preda, A quantum adiabatic evolution algorithm applied to random instances of an np-complete problem, Science **292**, 472 (2001).

[3] Wim Van Dam, Michele Mosca, and Umesh Vazirani, in *Proceedings 2001 IEEE International Conference on Cluster Computing* (IEEE, Las Vegas, Nevada, USA, 2001), p. 279.

[4] Tameem Albash and Daniel A. Lidar, Adiabatic quantum computation, Rev. Mod. Phys. **90**, 015002 (2018).

[5] D. Aharonov, W. Van Dam, J. Kempe, Z. Lamda, S. Lloyd, and O. Regev, in *Proceedings of the 45th IEEE Symposium on Foundations of Computer Science, Rome, Italy* (IEEEE, Rom, Italy, 2004), p. 42.

[6] Sergey Bravyi, David P. DiVincenzo, Daniel Loss, and Barbara M. Terhal, Quantum Simulation of Many-body Hamiltonians Using Perturbation Theory with Bounded-strength Interactions, Phys. Rev. Lett. **101**, 070503 (2008).

[7] Walter Vinci and Daniel A. Lidar, Non-stoquastic hamiltonians in quantum annealing via geometric phases, npj Quantum Inf. **3**, 38 (2017).

[8] Andrew J. Kerman, Superconducting qubit circuit emulation of a vector spin-1/2, New J. Phys. **21**, 073030 (2019).

[9] Dorit Aharonov, Wim Van Dam, Julia Kempe, Zeph Landau, Seth Lloyd, and Oded Regev, Adiabatic quantum computation is equivalent to standard quantum computation, SIAM Rev. **50**, 755 (2008).

[10] V. Efimov, Weakly-bound states of three resonantly-interacting particles, Sov. J. Nucl. Phys. **12**, 101 (1971).

[11] T. Kraemer, M. Mark, P. Waldburger, J. G. Danzl, C. Chin, B. Engeser, A. D. Lange, K. Pilch, A. Jaakkola, and H.-C. Nägerl *et al.*, Evidence for efimov quantum states in an ultracold gas of caesium atoms, Nature **440**, 315 (2006).

[12] Stephen P. Jordan and Edward Farhi, Perturbative gadgets at arbitrary orders, Phys. Rev. A **77**, 062329 (2008).

[13] Nicholas Chancellor, Stefan Zohren, and Paul A. Warburton, Circuit design for multi-body interactions in supercon-

ducting quantum annealing systems with applications to a scalable architecture, npj Quantum Inf. **3**, 21 (2017).

[14] Martin Leib, Peter Zoller, and Wolfgang Lechner, A transmon quantum annealer: Decomposing many-body ising constraints into pair interactions, Quantum Sci. Technol. **1**, 015008 (2016).

[15] J. E. Mooij, T. P. Orlando, L. Levitov, Lin Tian, Caspar H. Van der Wal, and Seth Lloyd, Josephson persistent-current qubit, Science **285**, 1036 (1999).

[16] Michel H. Devoret, Quantum fluctuations in electrical circuits, Les Houches, Session LXIII 7 (1995).

[17] E. K. Irish, J. Gea-Banacloche, I. Martin, and K. C. Schwab, Dynamics of a two-level system strongly coupled to a high-frequency quantum oscillator, Phys. Rev. B **72**, 195410 (2005).

[18] Pei-Qing Jin, Michael Marthaler, Alexander Shnirman, and Gerd Schön, Strong Coupling of Spin Qubits to a Transmission Line Resonator, Phys. Rev. Lett. **108**, 190506 (2012).

[19] J. R. Schrieffer and P. A. Wolff, in *Selected Papers Of J Robert Schrieffer: In Celebration of His 70th Birthday* (World Scientific, Singapore, 2002), p. 371.

[20] Sergey Bravyi, David P. DiVincenzo, and Daniel Loss, Schrieffer–wolff transformation for quantum many-body systems, Ann. Phys. (N. Y.) **326**, 2793 (2011).

[21] M. Born and R. Oppenheimer, Zur quantentheorie der molekeln, Ann. Phys. **389**, 457 (1927).

[22] Dvir Kafri, Chris Quintana, Yu Chen, Alireza Shabani, John M. Martinis, and Hartmut Neven, Tunable inductive coupling of superconducting qubits in the strongly nonlinear regime, Phys. Rev. A **95**, 052333 (2017).

[23] M. G. Castellano, F. Chiarello, P. Carelli, C. Cosmelli, F. Mattioli, and G. Torrioli, Deep-well ultrafast manipulation of a squid flux qubit, New J. Phys. **12**, 043047 (2010).

[24] Andrew Kerman, in *APS Meeting Abstracts* (APS, Los Angeles, California, USA, 2018).

[25] Denis Melanson, Antonio J. Martinez, Salil Bedkihal, and Adrian Lupascu, Tunable three-body coupler for superconducting flux qubits, arXiv:1909.02091 (2019).

[26] M. H. S. Amin, Flux qubit in charge-phase regime, Phys. Rev. B **71**, 024504 (2005).

[27] E. Paladino, Y. M. Galperin, G. Falci, and B. L. Altshuler, $1/f$ noise: Implications for solid-state quantum information, Rev. Mod. Phys. **86**, 361 (2014).

[28] Radoslaw C. Bialczak, R. McDermott, M. Ansmann, M. Hofheinz, N. Katz, Erik Lucero, Matthew Neeley, A. D. O'Connell, H. Wang, A. N. Cleland, and John M. Martinis, $1/f$ Flux Noise in Josephson Phase Qubits, Phys. Rev. Lett. **99**, 187006 (2007).

[29] Wolfgang Lechner, Philipp Hauke, and Peter Zoller, A quantum annealing architecture with all-to-all connectivity from local interactions, Sci. Adv. **1**, e1500838 (2015).